2009-01-01

Experimental Investigation of a Meso-Scale Axial Flow Pump

Jonathon Ray Bice
University of Texas at El Paso, jrbice@miners.utep.edu

EXPERIMENTAL INVESTIGATION OF A MESO-SCALE AXIAL FLOW PUMP

JONATHON RAY BICE

Department of Mechanical Engineering

APPROVED:

Ahsan Choudhuri, Ph.D., Chair

John F. Chessa, Ph.D.

Eric MacDonald, Ph.D.

Patricia D. Witherspoon, Ph.D.
Dean of the Graduate School

Dedication

I would like to dedicate this work to my family.

EXPERIMENTAL INVESTIGATION OF A MESO-SCALE AXIAL FLOW PUMP

by

JONATHON RAY BICE, B.S. Mechanical Engineering

THESIS

Presented to the Faculty of the Graduate School of

The University of Texas at El Paso

in Partial Fulfillment

of the Requirements

for the Degree of

MASTER OF SCIENCE

Department of Mechanical Engineering

THE UNIVERSITY OF TEXAS AT EL PASO

August 2009

Acknowledgements

Would like to acknowledge the entire UTEP faculty and staff who have helped me achieve the goal of earning degrees in higher education. It was a great honor learning from every one of you, and I hope to one day pass that knowledge and more onto others. I would also like to acknowledge the research assistants of the Combustion and Propulsion Research Lab (CPRL). Their tireless efforts have been an invaluable asset to the success of this project. I also express by deep gratitude to Dr. Ahsan Choudhuri, leader of the CPRL. Thank you for allowing me the opportunity to work in your lab and do my part to advance its research efforts.

Of course I save the most important for last. To my wife Blanca…You kept me going even when I couldn't find it in myself to do it. Thank you for all your support

Abstract

The scope of this work involves the testing of an experimental meso-scale axial flow pump intended for use in micro-spacecraft and micro-satellites. A setup was implemented to test pressure and flow characteristics at different velocities for three configurations of the pump. In addition, an alternate setup was used to test torque and efficiency. Computational fluid dynamics simulations were also conducted. The results are presented and analyzed to determine whether the pump is a viable alternative for the space industry.

Table of Contents

List of Tables

List of Figures

List of Illustrations

Nomenclature

Symbol	Definition	Units
bhp	brake horsepower	W
g	gravity	m/s^2
$h_{L,total}$	total irreversible head loss	m
$h_{pump,u}$	useful pump head	m
$\dot{m}$	mass flow	kg/s
p	pressure	Pa
p_v	saturation pressure	Pa
z	height	m
C_H	head coefficient	dimensionless
C_Q	capacity coefficient	dimensionless
C_P	power coefficient	dimensionless
D	diameter	m
H	net head	m
$H_{required}$	required net head	m
I	current	A

NPSH	net positive suction head	m
P	power	W
$T_{predicted}$	predicted torque	N-m
T_{shaft}	shaft torque	N-m
U	velocity	m/s
V	voltage	V
$\dot{V}$	volumetric flow	m^3/s
$\dot{W}_{water\ horsepower}$	water horsepower	W
$\dot{W}_{shaft}$	shaft power	W
$\eta_{predicted}$	predicted efficiency	%
η_{pump}	pump efficiency	%
ρ	density	kg/m^3
ω	angular velocity	rpm

Chapter 1: Introduction

A pump is a device used to transport a fluid. Since the initial development of the pump in the early 200's B.C., many different variations have been designed according to some specific purpose. However, all pumps can all be categorized into two basic types: positive displacement and rotodynamic. Positive displacement pumps work by directing fluid into a closed volume and adding energy to the fluid by means of a moving boundary. Rotodynamic pumps use rotating blades to increase the energy of the fluid. Rotodynamic pumps driven by a shaft are known as turbo-pumps [1].

The scope of this work involves the testing of an experimental meso-scale axial flow turbo-pump being developed for space applications. Meso-scale means that all pump component dimensions are in the millimeter range. Axial flow pumps are designed to produce high flow rates at lower pressures.

In current spacecraft research, there is a growing need for the standardization and miniaturization of spacecraft components. Current technology calls for customized spacecraft hardware as dictated by the needs of the mission. Size is also a limiting factor in mission cost because the bulk of mission cost is dominated by the cost of launching a spacecraft and inserting it into orbit. In most cases, only a single spacecraft can be placed on a launch vehicle for insertion into orbit. However, if spacecraft mass and size are reduced, smaller launch vehicles or multiple spacecraft per launch vehicle can be achieved. This enables in the reduction of transportation, manufacturing, and operational costs.

The experimental meso-scale axial flow pump under discussion is intended as a component for a meso-scale spacecraft liquid propulsion system. Liquid propellant turbo-pump fed propulsion systems offer superior performance and higher thrust-to-weight ratios. Miniature liquid propulsion engines using a turbo-pump feed system face limitations due to the development of a suitable meso-scale turbo-pump. Such limitations, including cavitation behavior, viscous effects, surface roughness, and alignment issues increase as the size of the pump decreases. This makes the scaling prediction difficult, particularly at the meso-scale. However, recent developments in machining technology make it possible to machine millimeter scale pump components with reasonable precision. Also, the development of meso-scale diagnostic techniques allows analysis of flow in millimeter-scale geometries. A unique and integrated

use of such technologies could lead the way to development of meso-scale turbo-pump technologies for use in smaller propulsion systems.

1.1 LITERATURE REVIEW

Current literature offer well developed theories for pump design and operation. Several equations are available to calculate various pump performance parameters as well as to design a pump. The key equations used to assist in the pump design are as follows:

The equation for net head is:

$$H = \left(\frac{p}{\rho g} + \frac{V^2}{2g} + z\right)_{out} - \left(\frac{p}{\rho g} + \frac{V^2}{2g} + z\right)_{in} \tag{1}$$

The equation for required net head is:

$$H_{required} = h_{pump,u} = \frac{p_2 - p_1}{\rho g} + \frac{U_2^2 - U_1^2}{2g} + (z_2 - z_1) + h_{L,total} \tag{2}$$

The net positive suction head is:

$$NPSH = \left(\frac{p}{\rho g} + \frac{V^2}{2g}\right)_{pump\ inlet} - \frac{p_v}{\rho g} \tag{3}$$

Several dimensionless parameters useful for pump design come from pump scaling laws. Although scaling prediction can be difficult at the meso-scale, the following dimensionless parameters can still provide a useful baseline from which to further improve design.

$$C_H = Head\ coefficient = \frac{gH}{\omega^2 D^2} \tag{4}$$

$$C_Q = Capacity\ coefficient = \frac{\dot{V}}{\omega D^3} \tag{5}$$

$$C_P = power\ coefficient = \frac{bhp}{\rho \omega^3 D^5} \tag{6}$$

$$N_{Sp} = pump\ specific\ speed = \frac{C_Q^{1/2}}{C_H^{3/4}} = \frac{\left(\dot{V}/\omega D^3\right)^{1/2}}{(gH/\omega^2 D^2)^{3/4}} = \frac{\omega \dot{V}^{1/2}}{(gH)^{3/4}} \tag{7}$$

1.2 PROJECT GOALS AND OBJECTIVES

The goal of this project is to develop a meso-scale axial flow pump suitable for use in meso-scale spacecraft and satellites. The design of the pump is based on well-established fluid mechanics principles regarding pump behavior as well as the use of scaling laws. Once the design has been selected, a prototype will be manufactured using suitable CNC mill and lathe technology. The prototype and alternate configurations of it will then be tested to experimentally determine the pressure and flow characteristics in order to validate intended design specifications. Throughout experiments, computational fluid dynamics (CFD) analyses will be conducted to validate experimental results and improve design as needed.

1.3 THESIS ORGANIZATION

The thesis is organized into seven chapters. The first chapter concerns stating the problem statement and establishing the design and testing requirements for a meso-scale axial flow pump. A brief description of the facility (in which the pump was developed and tested) and its capabilities is presented as well. The second chapter provides a description of the design requirements and processes undertaken to develop a suitable prototype. A brief description of alternate configurations that were tested is also discussed. The third chapter describes the experimental setups and the equipment required to determine pump performance characteristics. The fourth chapter presents the experimental data regarding pressure and flow rate with an analysis of cavitation. The fifth chapter presents the data used to measure power and torque characteristics. The sixth chapter details CFD procedures and analysis. Finally, the seventh and last chapter detail recommendations for future experimental work and final conclusions.

1.4 COMBUSTION AND PROPULSION RESEARCH LAB

Experiments on the meso-scale axial flow pump were performed in the Combustion and Propulsion Research Laboratory (CPRL) located in the Engineering Building of the University of Texas at El Paso (UTEP). The CPRL's primary research is in the areas of micro-propulsion and micro-combustion for the Departments of Defense and Energy. A wide variety of sensors, optical instrumentation, and data acquisition equipment, facilities, as well as computer software for modeling and simulations provide are available for use. The lab also has its own facilities for manufacturing prototypes and specialty equipment without much need for outsourcing.

Chapter 2: Pump Design

The experimental axial flow turbo-pump was developed by researchers at the CPRL. The intent was to develop a means of liquid fuel and oxidizer delivery to meso-scale propulsion systems for use in ballistic missile defense and meso-scale satellite technology. It should be noted that the author of this work only tested the prototypes and was not directly involved the design process. However, it is important to briefly describe the design process from conception to prototype development.

Although the pump is intended for use in micro-propulsion applications for use in space, its possibilities are not limited to only these applications. Other possible applications include a means for cooling electronics or for use in cardio assistive devices in the medical field.

2.1 PUMP PARAMETERS

Certain criteria were needed to design a pump suitable to the desired applications. The equations stated in the previous chapter provided the foundation under which the design process began. Investigating the needs of meso-scale rocket engines also being developed in the CPRL, a maximum discharge pressure was required to be 2MPa (20bar) with an inlet pressure of 0.6MPa (6bar). The working fluid around which the pump was designed was ethanol with a density of 789kg/m^3 and vapor pressure p_v of 15.9kPa (0.159 bar). The designed flow rate was 70mL/s. Table 2.1 is a summary of the design parameters.

Table 2.1: Design Parameters for Axial Flow Pump

Propellant	Ethanol, N_2O_4, MMH
Pressure Rise	20-100bar (2-10MPa)
Inlet Pressure	6bar (0.6MPa)
Throttling Range	50-90mL/s
Propellant Flow Rate	70mL/s

2.2 PUMP PROPERTIES

Using the equations from Section 1.1, a final pump design was selected, after several iterations. A NPSH of 75m was determined for a single-stage with a maximum rotational speed of approximately 220,000rpm. This required the impeller section to have a linear velocity of 80m/s with a tip diameter of 6.89mm and hub diameter of 3.49mm.

Three components were designed. The first component was the inlet guide vanes (IGV) to help guide and straighten the flow before going into the impeller stage. The rotor (also known as the impeller) increased the flow velocity to the desired level by means of four equi-axed rotating vanes. The third and final component is the four-vaned stator which reduced flow velocity and increased fluid pressure. The IGV and stator are both stationary. All had hub diameters of 3.5mm and tip diameters of 7mm except for the rotor which has a tip diameter of 6.95mm. The tip diameter for the rotor was reduced to provide sufficient clearance between the tips of the rotor vanes and inner casing wall. Once the final designs for each component were chosen, the pump components were modeled using 3-D modeling software.

2.3 CAD/CAM

Unigraphics NX-4 was used to develop a 3-D model of each pump component: IGV, rotor and stator. Figure 2.1 is an image of the pump modeled from the CAD software. The same program was also used to generate the G-code needed for manufacturing pump parts via CNC mill and CNC lathe. Initial prototypes were made using acrylic but testable pump components were manufactured from Al 6061 aluminum alloy. Aluminum alloy was chosen for ease of machining as well as for its weight characteristics. The bearings used for the pump are double shielded, ABEC-5, stainless steel ball bearings. Future pump prototypes to be tested will be made of Ti-Al6V4 titanium alloy. Although it can be difficult to machine, the material is an excellent option for its excellent strength to weight properties.

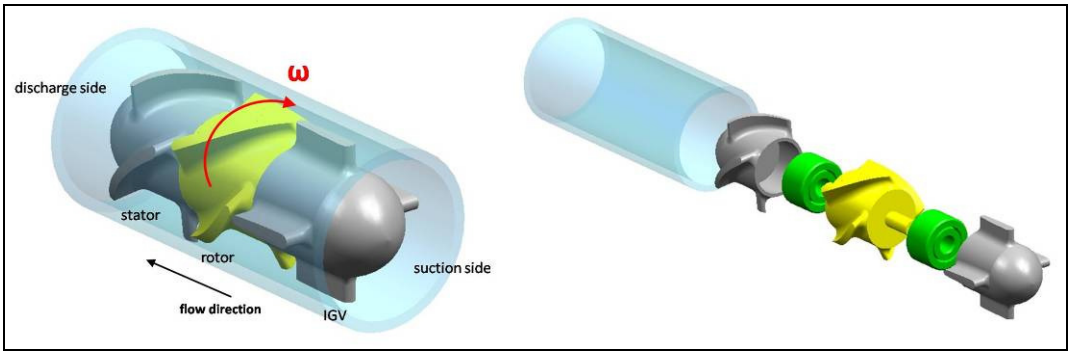

Figure 2.1: CAD Model of Experimental Axial Flow Pump with Exploded View.

2.4 OTHER CONFIGURATIONS

Two alternate pump configurations were prototyped and tested to determine if they would match or enhance the design requirements of the original single stage prototype. One alternate configuration consisted of the single stage axial flow pump with the casing modified to include a volute chamber (Figure 2.2). The idea was to increase discharge pressure using the expanding cross-sectional area of a volute similar to those found on centrifugal pumps. The second configuration (Figure 2.3) was to modify the single-stage axial flow pump to a two-stage axial flow pump. An additional rotor and modified stator (first stage stator) were added. Both rotors rotate at the same velocity.

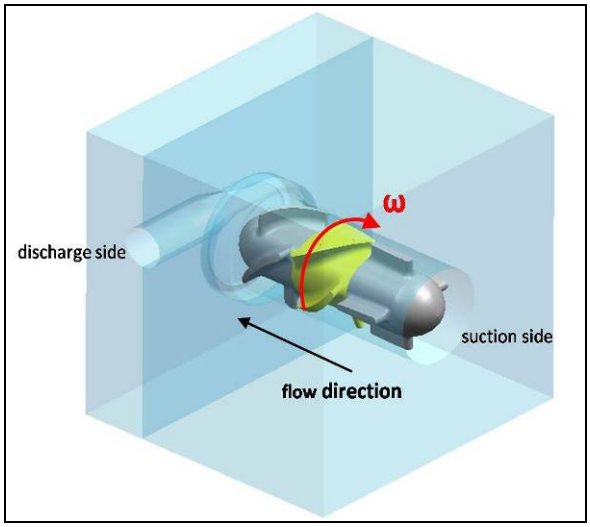

Figure 2.2: CAD Model of Volute Configuration.

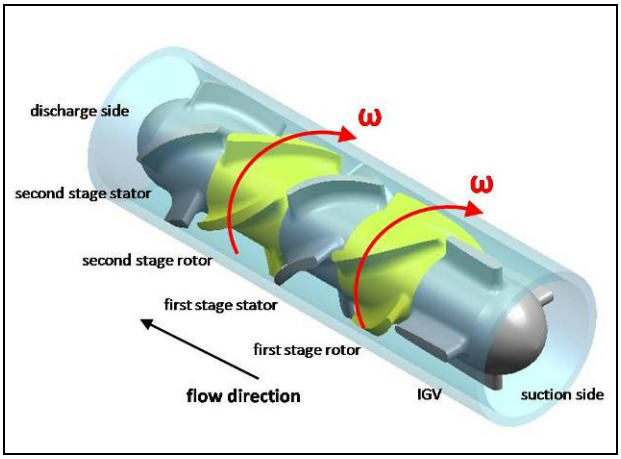

Figure 2.3: CAD Model of Experimental Axial Flow Pump.

Chapter 3: Experimental Setup

Multiple setups were required to test pump performance. One setup was used to measure flow and discharge pressure. A second was used to measure pump power. Power measurements were later used to calculate torque and efficiency. A third setup was constructed to demonstrate pump performance when coupled to an injector body. A description of the injector is given in section 4.3.

3.1 PUMP TEST SETUP

The experimental setup to measure discharge pressure and flow can be seen in Figure 3.1. It was designed to minimize the use of fittings as much as possible in order to minimize frictional and viscous losses. It was also designed so that a quick and simple change out of damaged or failed components was possible. It consisted of a closed loop system with two 90° radius bends and with measurement devices inserted as close as possible to the pump at its discharge end. A suction tank and a discharge tank were used to supply and recover the fluid as it was pumped across the system. A line connecting the suction tank and discharge tank maintained the fluid level in the suction tank at a constant level, thus maintaining a constant inlet pressure. Although both tanks had covers to help keep external contaminants out, the tanks were not sealed and were open to the atmosphere.

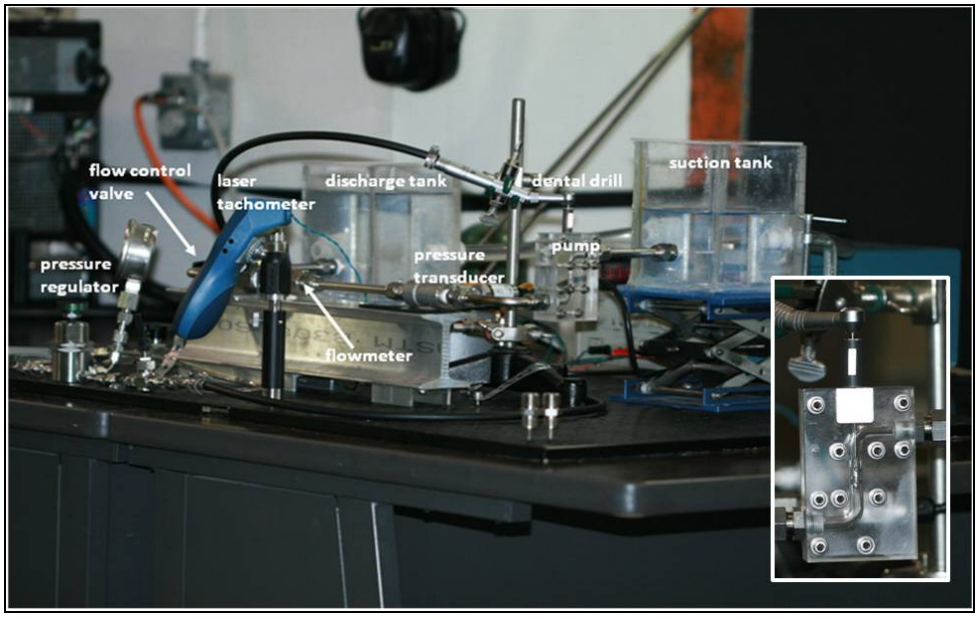

Figure 3.1: Pump Test Setup to Measure Flow Rate and Discharge Pressure.

Diagnostic devices were installed in the setup to record data from the experiments. An Omega Inc. pressure transducer (serial #122507D66) with a range of 0-500psig with a linear output of 0-5V was used to measure discharge pressure. Flow rate was measured with an Omega Inc. FTB-9504 turbine flowmeter (serial #259234) with a frequency output and a range of 50-1000mL/min. An Omega Inc. FLSC-61 signal conditioner (serial #29568) was used to convert the frequency output of the flowmeter into a voltage output. All voltage output signals were sent to a National Instruments Data Acquisition (NI-DAQ) device. A computer running the program LABVIEW was used to process the voltage output signals and record them for later processing. A Monarch PLT200 contact/noncontact laser tachometer (serial #1828075) with a noncontact range of 5-200,000rpm was used to measure pump rotational velocity. Figures 3.2 through 3.8 are images of the equipment used.

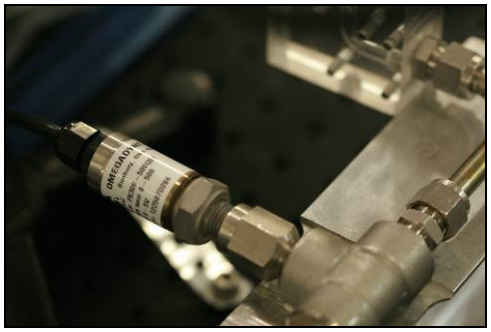

Figure 3.2: Pressure Transducer

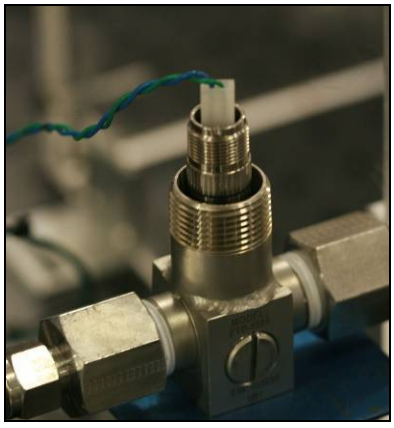

Figure 3.3: Turbine Flowmeter

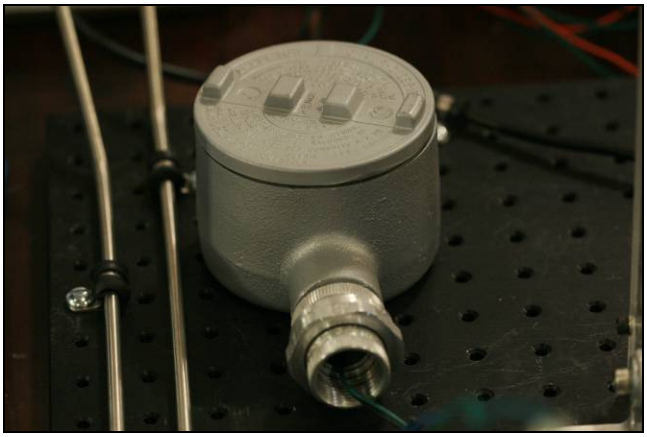

Figure 3.4: Signal Conditioner

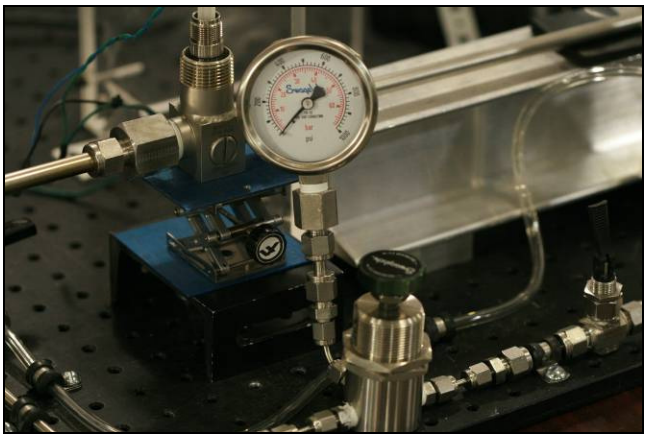

Figure 3.5: Pressure Control Valve Used for Controlling Pump Velocity

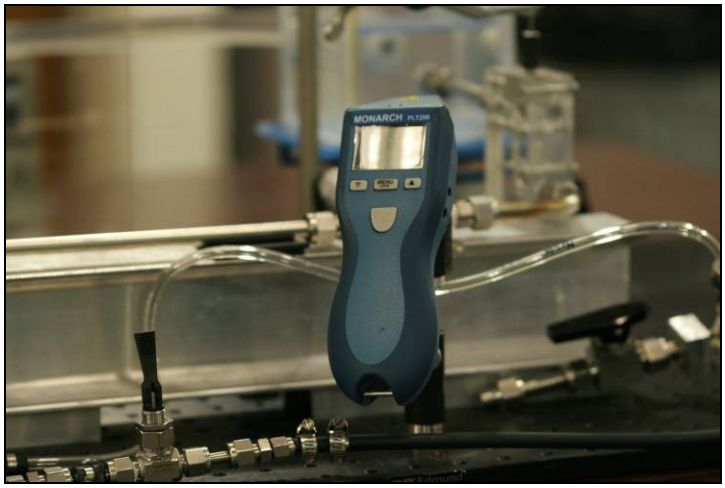

Figure 3.6: Laser Tachometer

Figure 3.7: Ni-DAQ Used for Data Acquisition

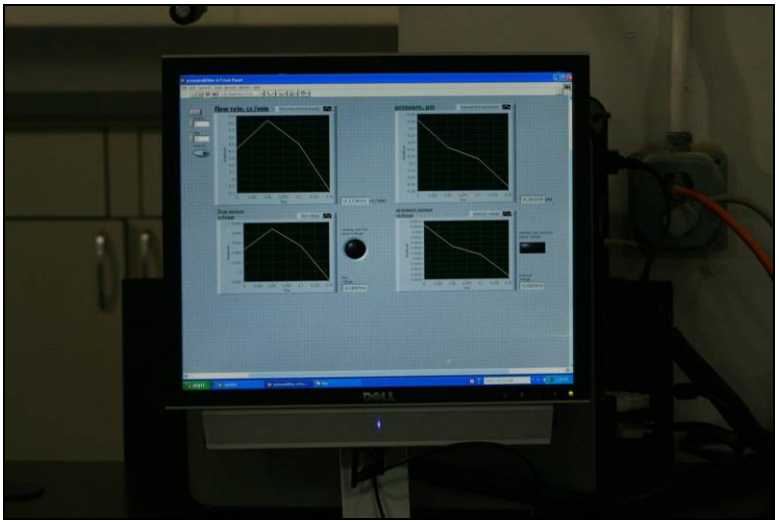

Figure 3.8: Computer with LABVIEW

The pump prototype was driven by a KaVo Inc 625C SuperTorque dental drill. Although the intended design of the experimental pump called for a motor to drive the impeller, one had not yet been developed. Therefore, the IGV component was modified with a through-hole along its axial direction to accommodate a through-shaft from the rotor coupled to the dental drill. Nitrogen gas was used to drive the drill and a pressure regulator used to control the dental drill speed. The pump was coupled to the dental drill using a 1.19mm stainless steel shaft fixed to the rotor, a black anodized 7.94mm aluminum rod and a 1.6mm high-speed steel drill blank. The drill blank was the exact diameter of burrs used for

the drill in conventional dental practice and coupled the pump to the drill nicely (see inset of Figure 3.1). The aluminum rod was used to couple the 1.19mm shaft to the drill blank. A thin strip of reflective tape was attached to the aluminum rod which reflected the laser from used by the tachometer to measure rotational velocity of the drill-pump setup. A Swagelok brand ¼ turn valve was used to manipulate flow.

To incorporate the pump into the closed loop system of the setup, a special casing needed to be manufactured. The casing was developed in NX-4 and was manufactured in two mirror image halves from 0.75in thick clear acrylic plate. This special casing also permitted the observer to visually examine pump performance during operation and record any still images or video using a still-frame or video camera. The casing and inserts were both machined using a Roland Modela 3-D printer. Figure 3.9 is a CAD representation and the actual image of the assembled casing with the experimental single-stage axial flow pump.

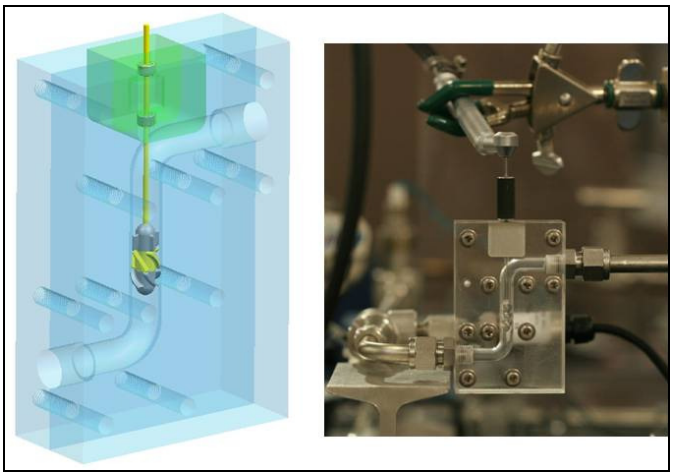

Figure 3.9: CAD model of modified pump casing used for experiments.

An aluminum insert (transparent green parts in CAD model in Figure 3.9) for the acrylic casing was needed to absorb frictional heat dissipated by the through-shaft, additional bearings and packing. Two shielded bearings were used to stabilize the 1.19mm shaft and mitigate excessive vibration because of its length and small diameter. The bearings are housed in the aluminum insert. Aluminum was chosen for ease of manufacture with the 3-D printer and because the frictional heat dissipation from the bearings would have melted the acrylic and seized the pump had only it been used. In between the

bearings, a chamber filled with high temperature silicon vacuum grease acted as packing to prevent fluid leaking from the system. Silicon grease was chosen because of its high temperature resistance properties and its resistance to dissolve into and contaminate the working fluid.

Distilled water was used as the working fluid as a starting point to observe pump performance. Approximately three liters of it were used in the experiment to fill the tanks and lines. Because the pump is very small, and the volume of water used was much greater by comparison, any temperature changes in the pump or water and thus density changes in the working fluid were considered negligible. In all tests, the temperature of the working fluid was 20°C ±0.5°C so the density was assumed to be 1000kg/m^3 [1]. In the future, other fuels and oxidizers, those characterized as earth-storable (i.e. hydrogen peroxide, liquid oxygen, and liquid hydrogen), will be used as working fluids to further develop and maximize pump design.

For the experimental procedure, the suction tank fluid level was 3in (0.076m) above the inlet to the pump. Thus pump inlet pressure was 3.48psi (24kPa). The pump was run at a constant angular velocity from 10,000-80,000rpm in increments of 10,000rpm with a fully open valve. Once steady state velocity had been reached the valve was slowly closed until shut. Free flow head to shutoff head were measured. Flow rate was also measured in this manner.

3.2 GENERATOR SETUP

In order to measure pump torque, an alternate setup was needed. A generator setup using a variable resistance load was set up to measure the voltage and current output (to calculate power) from the mechanical work of the dental drill. The results would be considered equivalent to which was considered equivalent to the power of the experimental pump. For this setup, a high speed 9-18 VDC motor was coupled to the dental drill. A motor converts electrical energy into mechanical energy. A device that uses the reverse process is called a generator. A 0-25Ω wirewound rheostat was installed in series for the variable load resistance. Two Fluke multimeters were use to measure voltage and current. One multimeter to measure voltage output from the setup was placed in parallel with the rheostat while a second multimeter to measure current was placed in series with the circuit. Illustration 3.1 shows a diagram of the circuit. Here, the ammeter measures the current while the voltmeter measures the voltage.

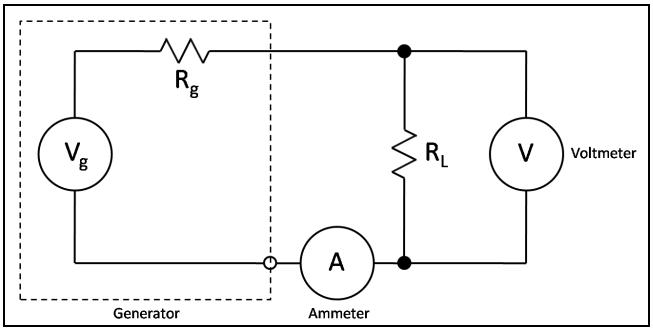

Illustration 3.1: Generator Test Setup Circuit Diagram.

The drill was run at a constant angular velocity at a range of 5,000-30,000rpm in intervals of 5,000rpm at a preset load resistance and current and voltage was measured. Increments of 1Ω±0.5Ω with a range of 3-6Ω were used. Voltage and current were measured three times for a given angular velocity and the averages taken. Figures 3.10 and 3.11 below show the experimental setup to test power.

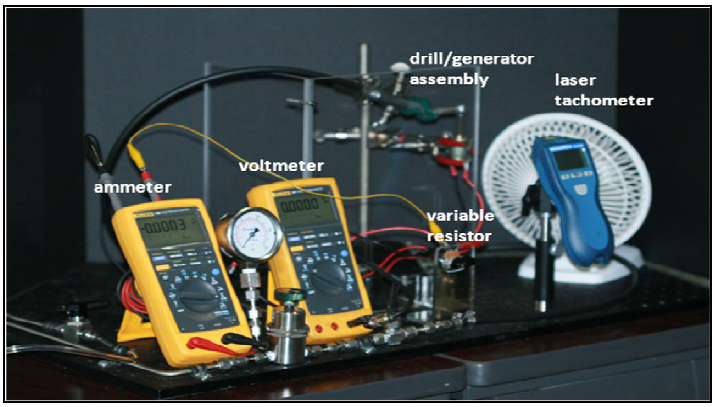

Figure 3.10: Generator Test Setup to Measure Power.

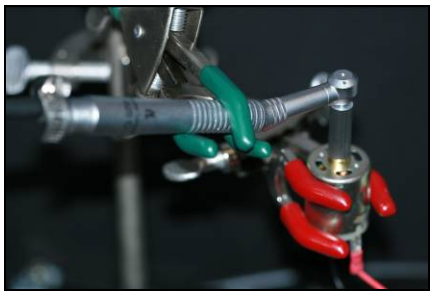

Figure 3.11: Detail View of Dental Drill/Generator Assembly.

Chapter 4: Pump Data Analysis

4.1 PUMP TEST RESULTS

4.1.1 Single Stage Axial Flow Pump

Inlet pressure was subtracted from discharge pressure measurements and the results were converted to pressure head from psi. Figure 4.1 is a plot of the pressure head as a function of flow rate along curves of constant angular velocity. For clarification of each curve, see Figure 4.2. As with results commonly found in published literature, maximum pressure head occurs at minimum flow rate and minimum pressure head occurs at maximum flow rate. Table 4.1 summarizes free flow pressure and shutoff head at a given angular velocity.

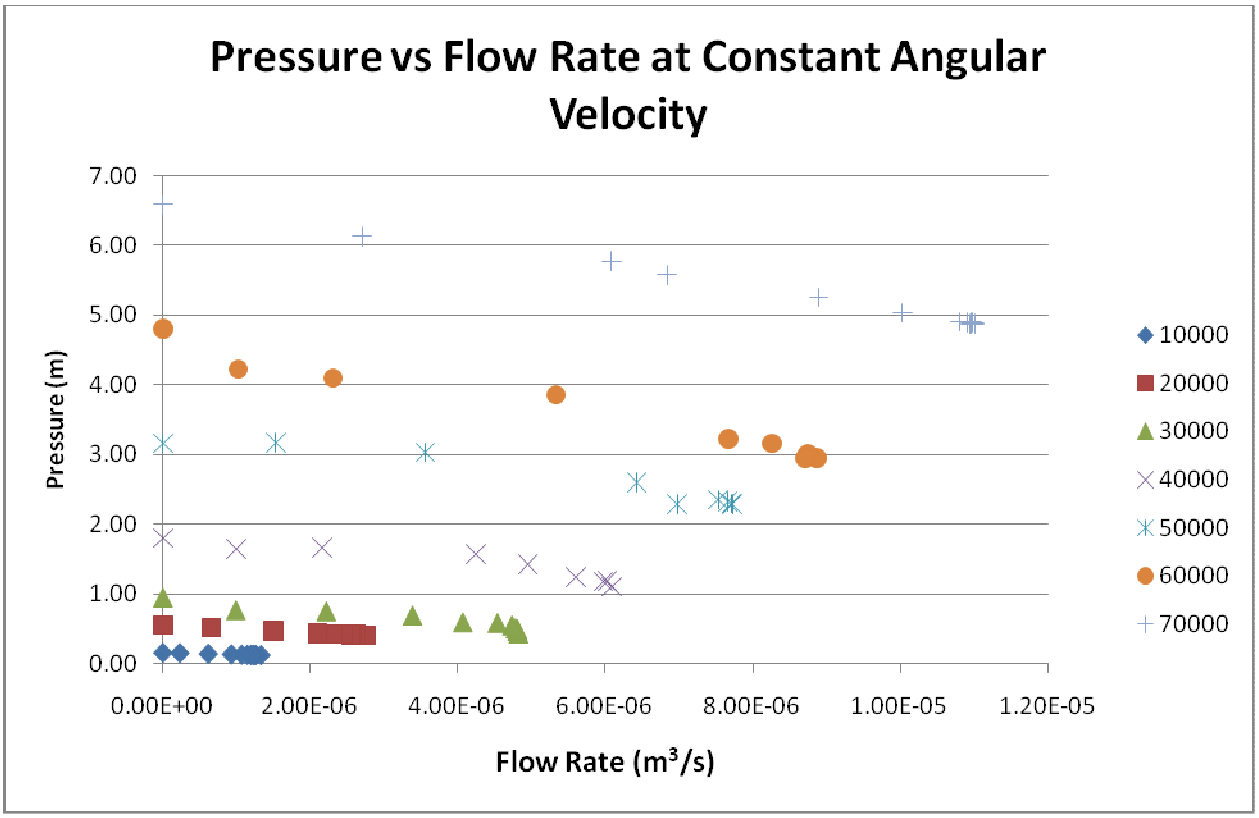

Figure 4.1: Combined Curves of Pressure Head vs. Flow Rate at Constant Angular Velocity.

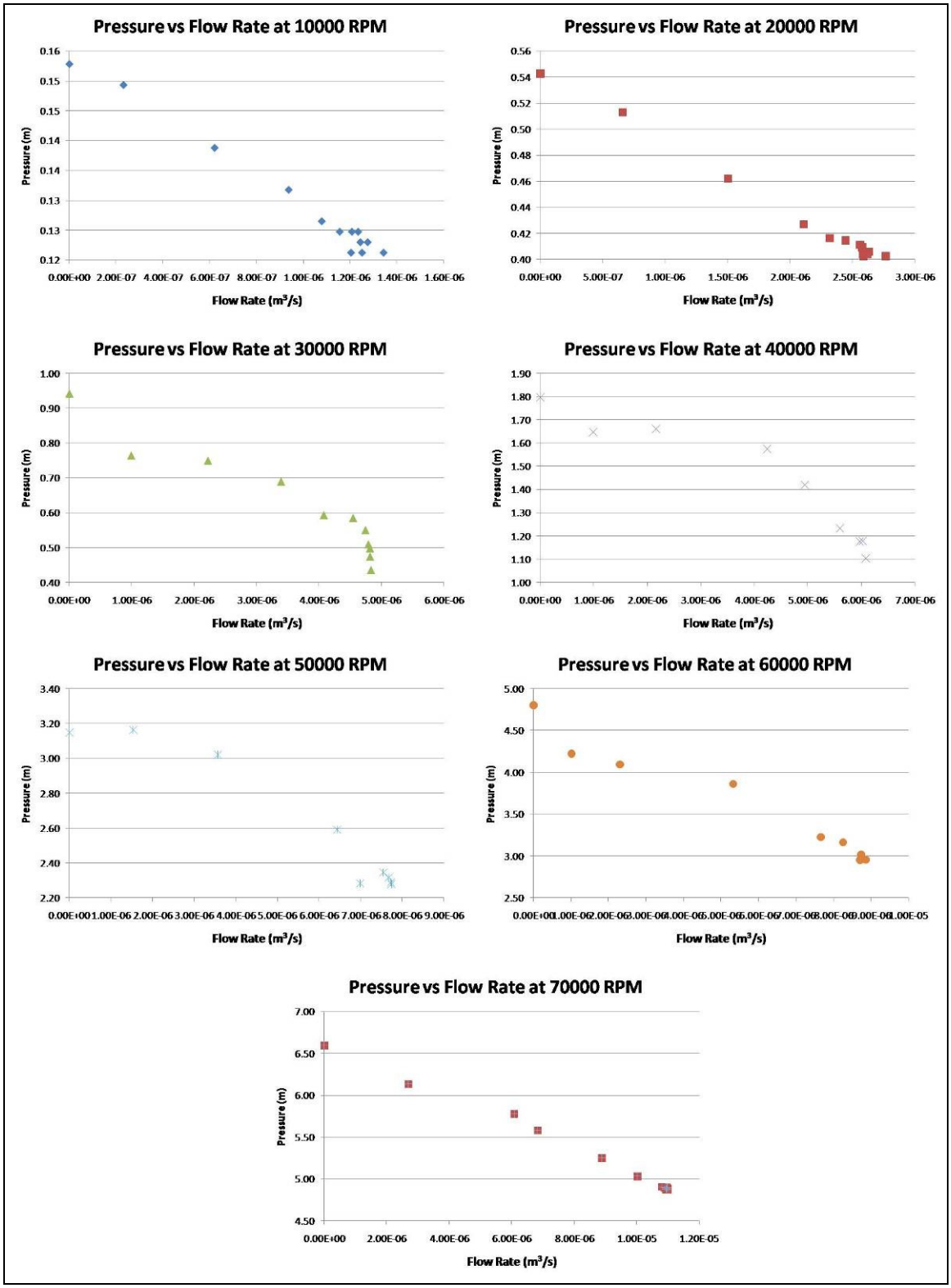

Figure 4.2: Pressure as a Function of Flow Rate at Constant Angular Velocity.

Table 4.1: Summary of Pressure Head and Free Flow Rate.

Angular Velocity (rpm)	Free Flow Rate (m^3/s)	Free Flow Head (m)	Shutoff Head (m)
10,000	1.34E-06	0.12	0.15
20,000	2.77E-06	0.40	0.54
30,000	4.83E-06	0.43	0.94
40,000	6.01E-06	1.10	1.80
50,000	7.73E-06	2.28	3.15
60,000	8.87E-06	2.95	4.81
70,000	1.10E-05	4.84	6.60

4.1.2 Single Stage Axial Flow Pump with Volute Casing

The results at 50,000rpm of the single stage axial flow pump with a modified volute casing are shown in Figures 4.3. According to the data, shutoff pressure head is 10.57m and free flow pressure head is 1.55m at a free flow velocity of $4.16x10^{-6}m^3/s$.

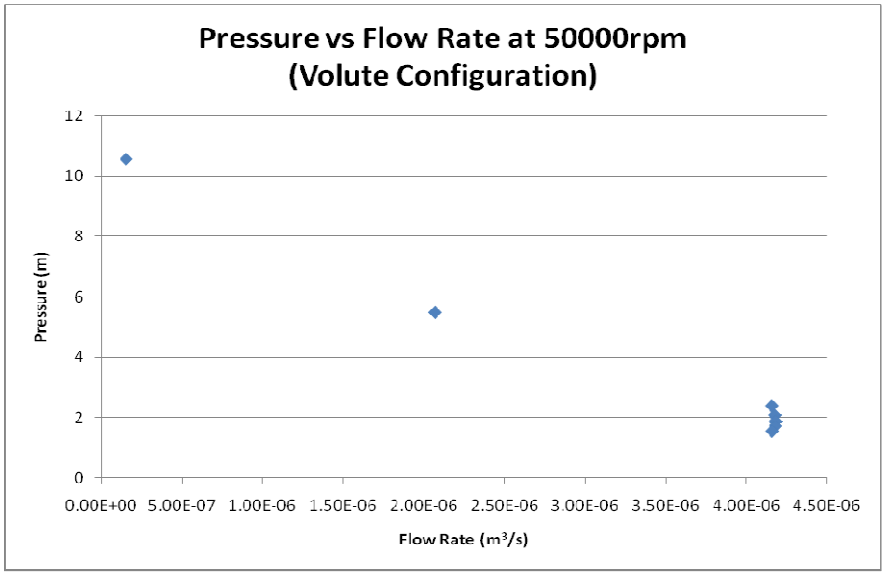

Figure 4.3: Pressure and Flow Rate Plot for Volute Configuration

4.1.3 Two-Stage Axial Flow Pump

The results of the two-stage axial flow pump are shown in Figure 4.4. It can be seen that shutoff pressure head is 7.69m and free flow pressure head is 6.81m at a free flow velocity of $6.55 \times 10^{-6} m^3/s$.

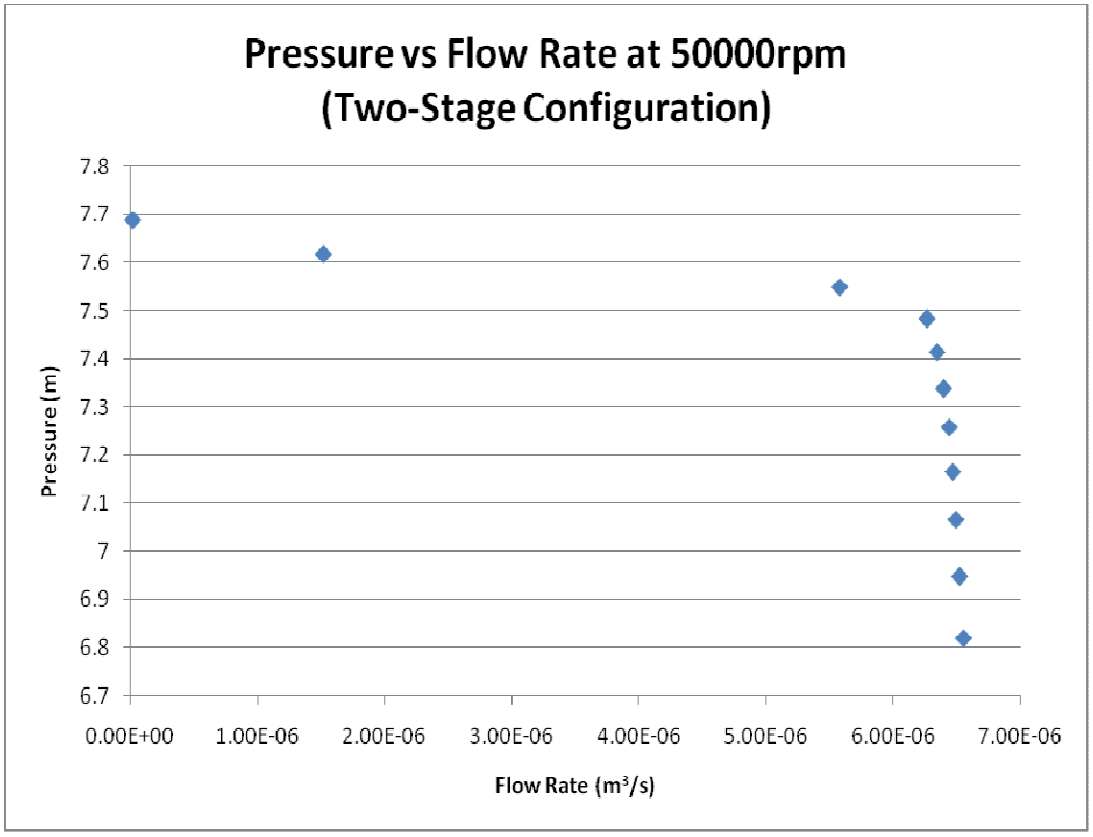

Figure 4.4: Pressure and Flow Rate Plot for Two-Stage Configuration

The two-stage configuration offers a higher free flow head when compared to the volute configuration and the standard configuration at the same angular velocity. However the volute produces the highest shutoff pressure head. Table 4.2 is a comparison of the three configurations at 50,000rpm. The standard configuration shows the best free flow rate. Figure 4.5 compares all three in a plot.

Table 4.2: Comparison of Three Pump Configurations at 50,000rpm

Configuration	Single Stage	Single-Stage Volute	Two-Stage
Free Flow Rate (m3/s)	7.73E-06	4.16E-06	6.55E-06
Free Flow Pressure (m)	2.28	1.55	6.82
Shutoff Pressure (m)	3.15	10.57	7.69

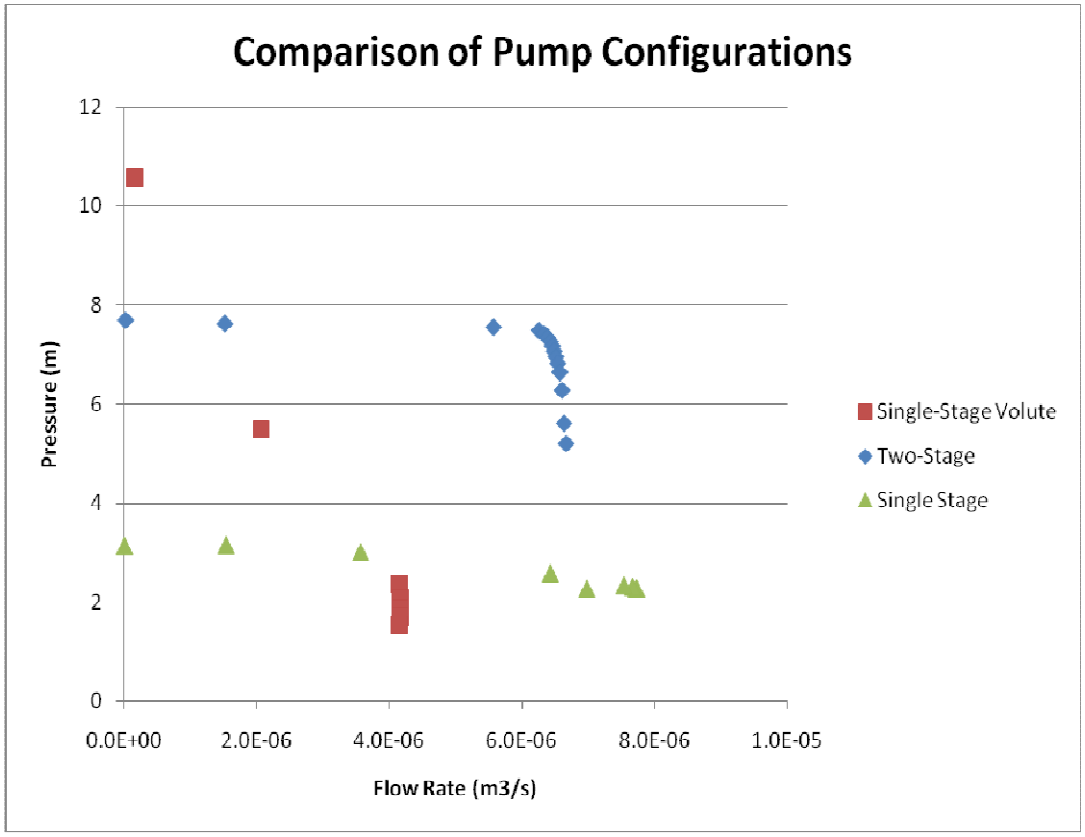

Figure 4.5: Comparison of Pump Configurations

4.2 CAVITATION

Cavitation is apparent when the pump is operating at 50000rpm and higher. To document cavitation phenomenon occurring at the inlet guide vanes, a Photron Fast Camera (FASTCAM) and a Canon single lens reflex (SLR) camera were used. Footage taken with the FASTCAM indicates bubble nucleation appears to begin just behind the leading edges of the IGV vanes. Cavitation further develops

upon passing across the IGV and once at the rotor, cavitation is further exacerbated. Beyond 75,000rpm, flow is completely choked and pressure and flow data cannot be determined. It is unclear if the rotating shaft passing through the IGV plays a factor in cavitation development. Considering viscous forces in the working fluid and the no-slip condition, the rotation of the shaft will cause the working fluid to rotate prior to entering the IGV. Figure 4.5 shows images of cavitation development taken with the SLR camera. What appears to be blurring in the images (highlighted by dotted white circles) is actually cavitation. Figure 4.5(a) is an image of the experimental pump at rest. Figure 4.5(b) shows cavitation development at 50,000rpm and Figure 4.5(c) show further cavitation occurring at 60,000rpm.

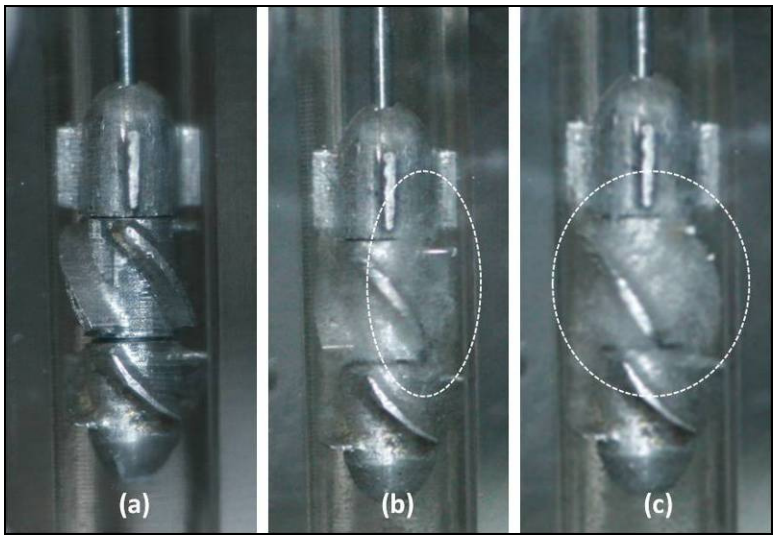

Figure 4.6: Cavitation images.

Figures 4.7 and 4.8 are a filmstrip of images of the experimental axial flow pump operating at 70,000rpm with the flow control valve at full open position. The images are taken from the FASTCAM at 5,000 frames per second. If the viewer follows the strip in order according to the frame number on the upper right of each image, one can see the cavitation development. It will appear as a blur in the image. Cavitation bubbles start just behind the leading edges of the inlet guide vanes and can be seen entering the rotor.

Figure 4.7: Cavitation images taken with the FASTCAM.

Figure 4.8: Cavitation images taken with the FASTCAM (continued).

4.3 OTHER ISSUES

During experiments, it was important to ensure the fluid lines in the setup contained no trapped air bubbles. This was especially true for bubbles located on the suction side of the pump. Observations during experimentation with only the rotor as well as the complete pump have shown that if a bubble approximately 1-2 mm diameter or greater enters into the suction side, the bubble becomes trapped in the rotor and flow becomes completely choked. Although not explicitly recorded, there were various occasions in which a bubble was observed to be drawn into the rotor or pump and flow effectively ceased until the bubble was removed. It is also likely that as the suction side pressure becomes closer to vapor pressure of a working fluid, it may take even smaller bubbles to choke flow or create an impetus for cavitation.

Another issue commonly observed during experiments was the tendency of air bubbles to stick to pump component surfaces. Those bubbles trapped on the IGV posed a greater risk of choking flow than those on the stator since bubbles on the IGV surface must still pass through to the rotor. Bubbles on the discharge side either remained attached to the stator or section walls or were ejected and removed upon entry into the discharge tank. Component surface finish after manufacture was the likely cause of bubble sticking to surfaces. A smoother finish would likely mitigate the problem.

4.3 DEMONSTRATION WITH AN INJECTOR BODY

The injector body is designed to atomize and mix the fuel and oxidizer before combustion. An injector plate is also added to the exit of the injector body but was not included for the experiment. A simplified CAD model is shown in Figure 4.8. The experimental setup is shown in Figure 4.9. A stand alone image of the front of the assembled injector body can be seen in Figure 4.10. A functional demonstration of the pump coupled to an injector body was conducted and still images are presented in Figure 4.11. Figure 4.11 shows the water-nitrogen gas mixture as it is exiting the injector body. 4.11(a) is for pump operation at 40,000rpm and nitrogen gas pressure 34.5kPa. For 4.11(b), the pump is operating at 30,000rpm and nitrogen gas pressure is at 206.8kPa. Distilled water acted as the fuel while nitrogen gas was used as the oxidizer. Larger water droplets can be observed in (a) as compared to (b). This is due to the lower nitrogen gas pressure used for the demonstration.

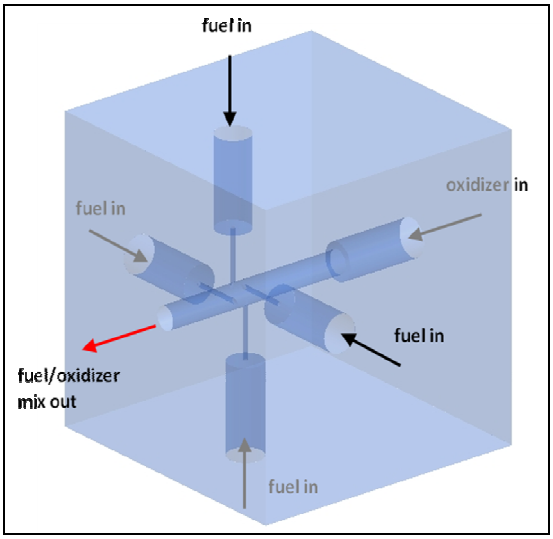

Figure 4.8: CAD Model of Injector Body.

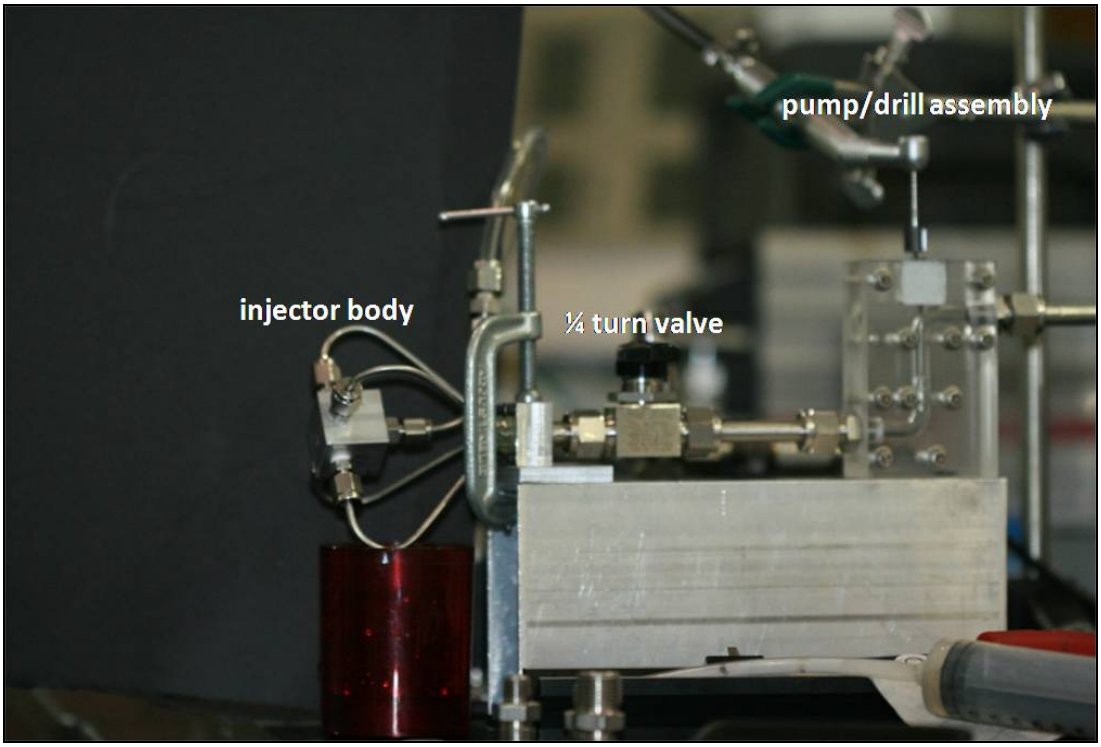

Figure 4.9: Pump-Injector Body Assembly Experimental Setup.

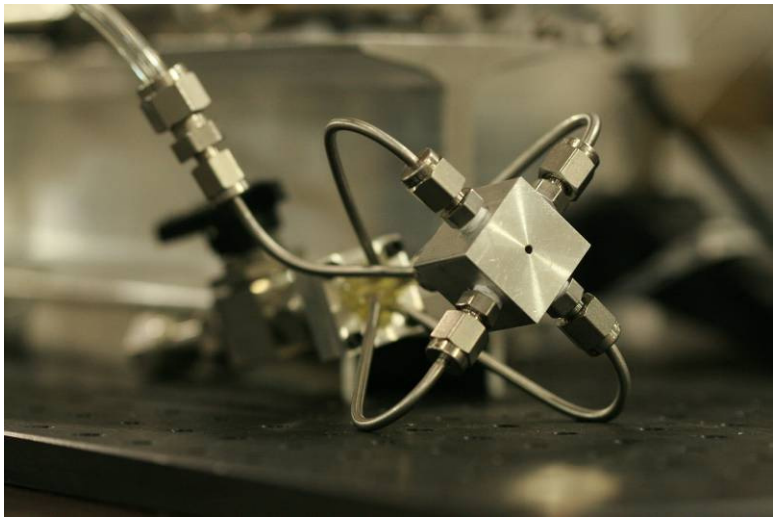

Figure 4.10: Front View of Assembled Injector Body.

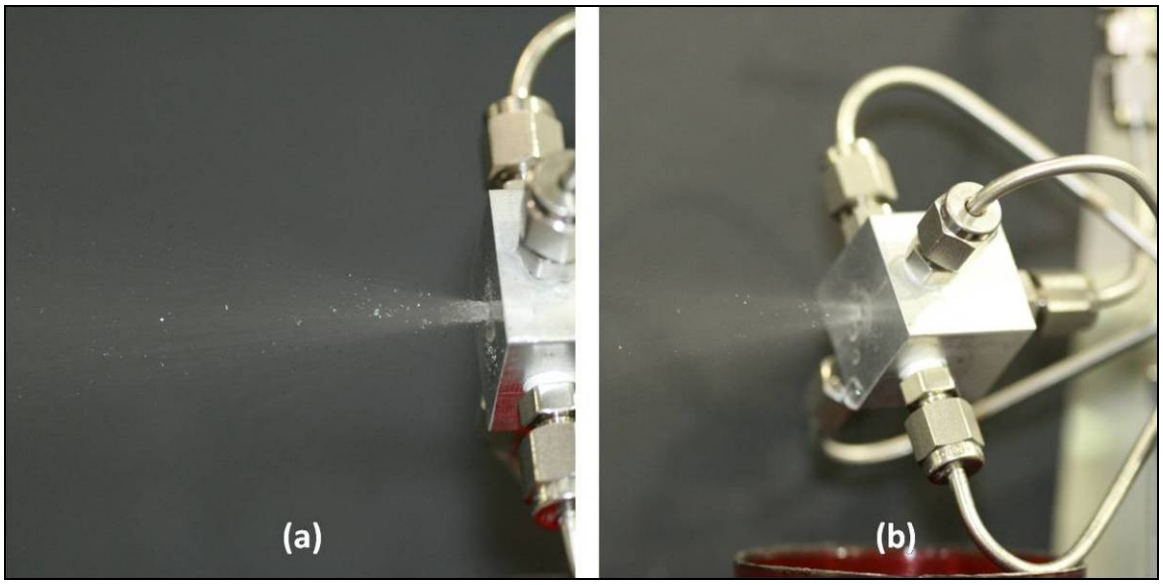

Figure 4.11: Pump-Injector Body Demonstration.

Chapter 5: Generator Data Analysis

5.1 Torque and Power Results

Power was calculated from the product of voltage and current output measurements. This is stated by the equation:

$$P = VI \tag{8}$$

The following figures are plots of power as a function of angular velocity. As angular velocity increases, power increases, however torque first increases rapidly but gradually begins to taper off following a logarithmic curve.

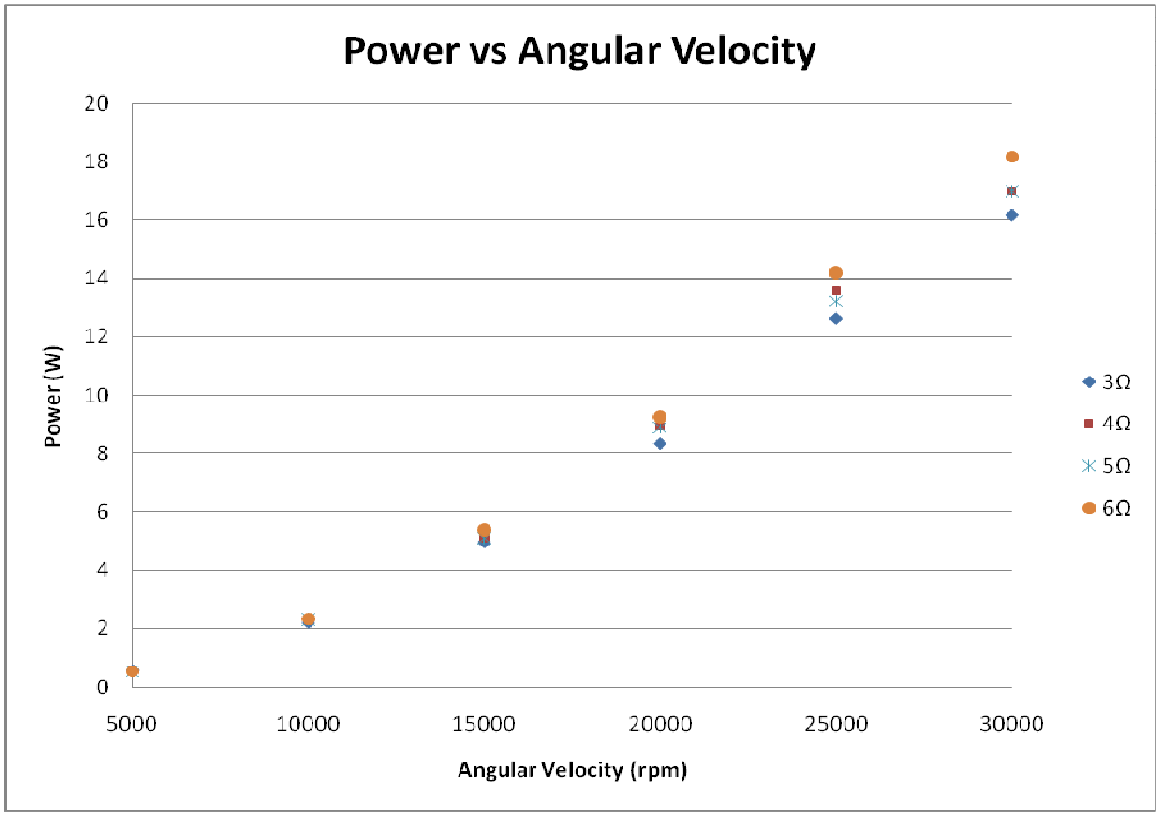

Figure 5.1: Power versus Angular Velocity.

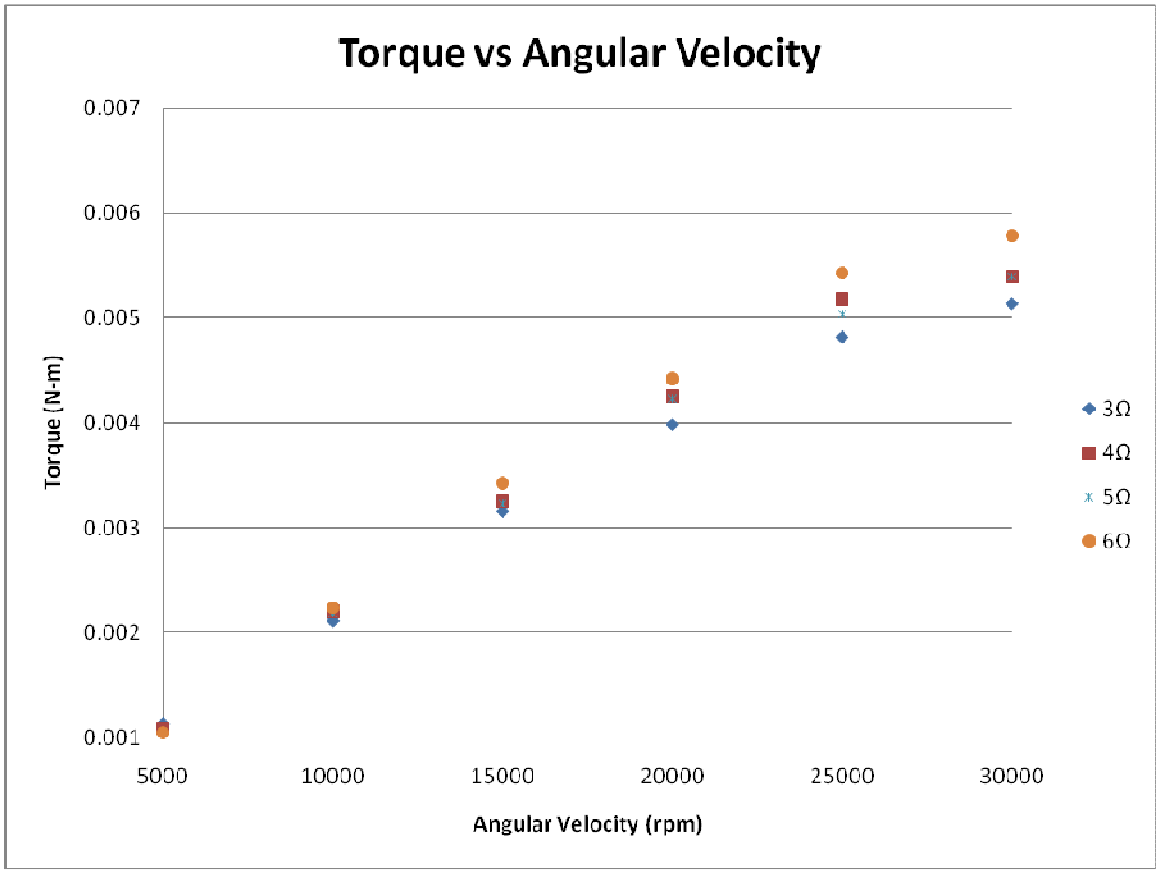

Figure 5.2: Torque versus Angular Velocity.

5.2 EFFICIENCY ANALYSIS

Efficiency was calculated using the following equations based on fluid mechanics principles:

$$\dot{W}_{water\ horsepower} = \dot{m}gH = \rho g\dot{V}H \tag{9}$$

$$bhp = \dot{W}_{shaft} = \omega T_{shaft} \tag{10}$$

$$\eta_{pump} = \frac{\dot{W}_{water\ horsepower}}{bhp} \tag{11}$$

$\dot{W}_{\text{water horsepower}}$ is the useful power delivered to the fluid by the pump. Brake horsepower, or bhp, is the power supplied to the pump. Equations (8) and (10) can be set equal to each other for the

purposes of the experiment since the power output by the drill/generator is the same as the power input of the pump to the working fluid. Only pressure and flow rate data for the single stage axial flow pump were used to compute torque and $\dot{W}_{\text{water horsepower}}$ and pump efficiency.

The dental drill was tested in the range of 5,000-30,000rpm during the generator experiment. A curve fit of the data (see Figure 5.3) yielded the following equation of torque as a function angular velocity:

$$T_{predicted} = 0.0023\ln(\omega) - 0.019 \tag{12}$$

The curve fit for Equation (12) had an R^2 value of 0.9724. A plot of actual torque and predicted torque yielded what is shown in Figure 5.4. At the maximum designed velocity, the predicted torque at 220,000rpm is expected to be 0.00995N-m.

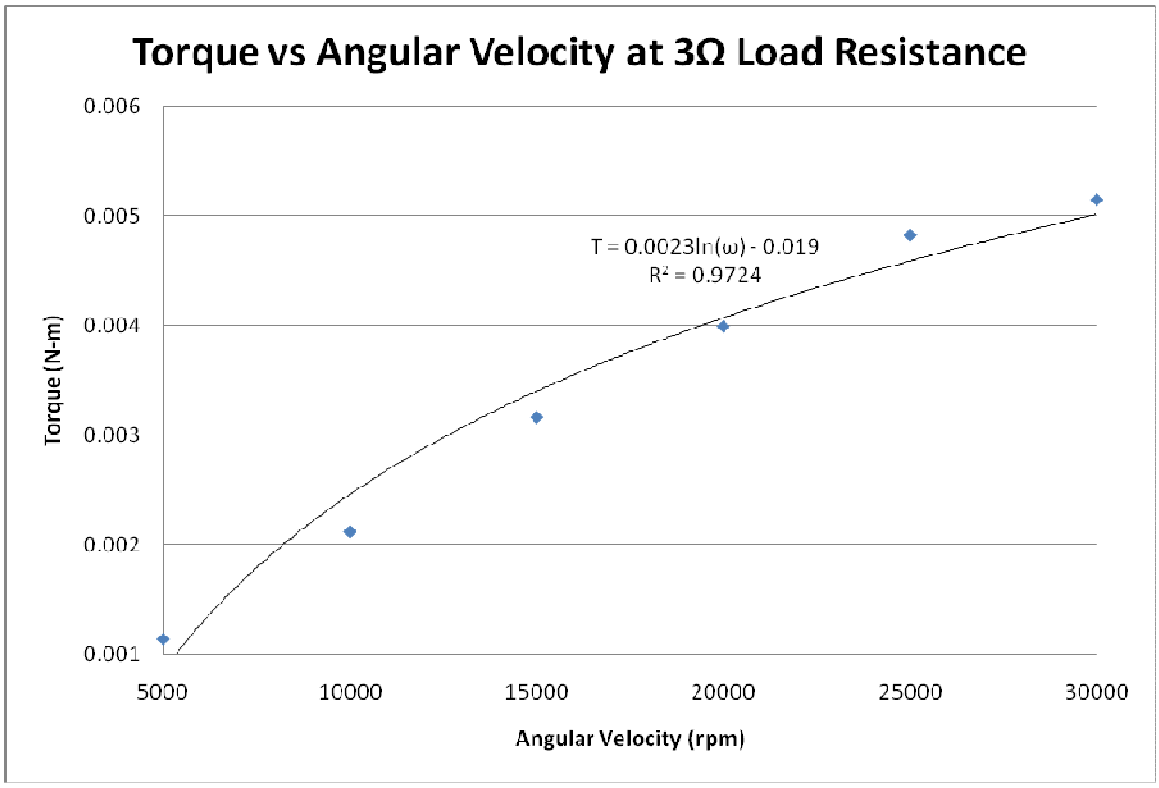

Figure 5.3: Torque versus Angular Velocity Curve Fit for 3Ω Load Resistance.

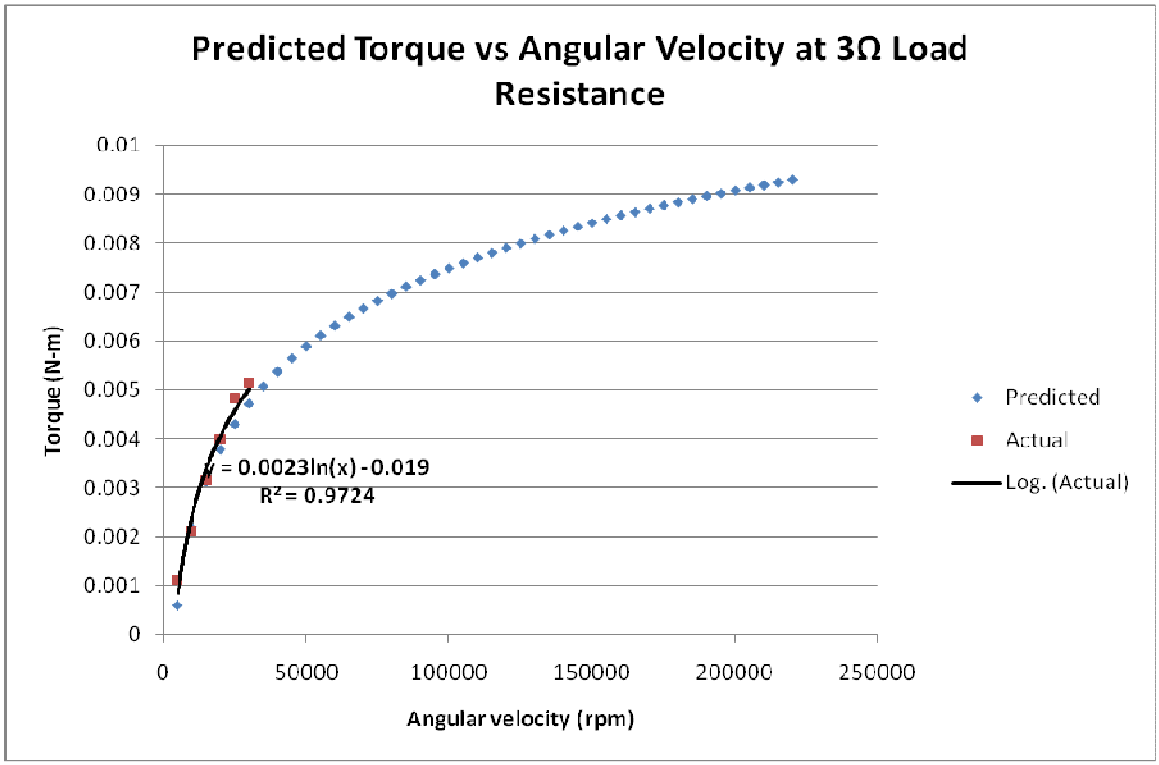

Figure 5.4: Predicted Torque versus Angular Velocity Curve Fit for 3Ω Load Resistance.

Plots of efficiency versus pressure head are shown in Figure 5.5. Individual plots are shown in Figure 5.7. It can be seen in all cases that as pressure head increases, efficiency decreases. Figures 5.6 and 5.8 are plots of efficiency versus flow rate. The figures indicate as flow rate increases, efficiency also increases.

The internal resistance in the circuit (see Figure 3.1) was greater than the actual frictional resistances in the pump. The drill/generator setup could not be safely pushed past 30,000rpm because the required pressures to operate the drill were well beyond its intended design limits. Adding the ammeter to the circuit further strained the dental drill to drive the generator. This is likely due to the internal shunt resistor that is part of the internal circuitry of the multimeter (ammeter) which is used to measure current across the circuit.

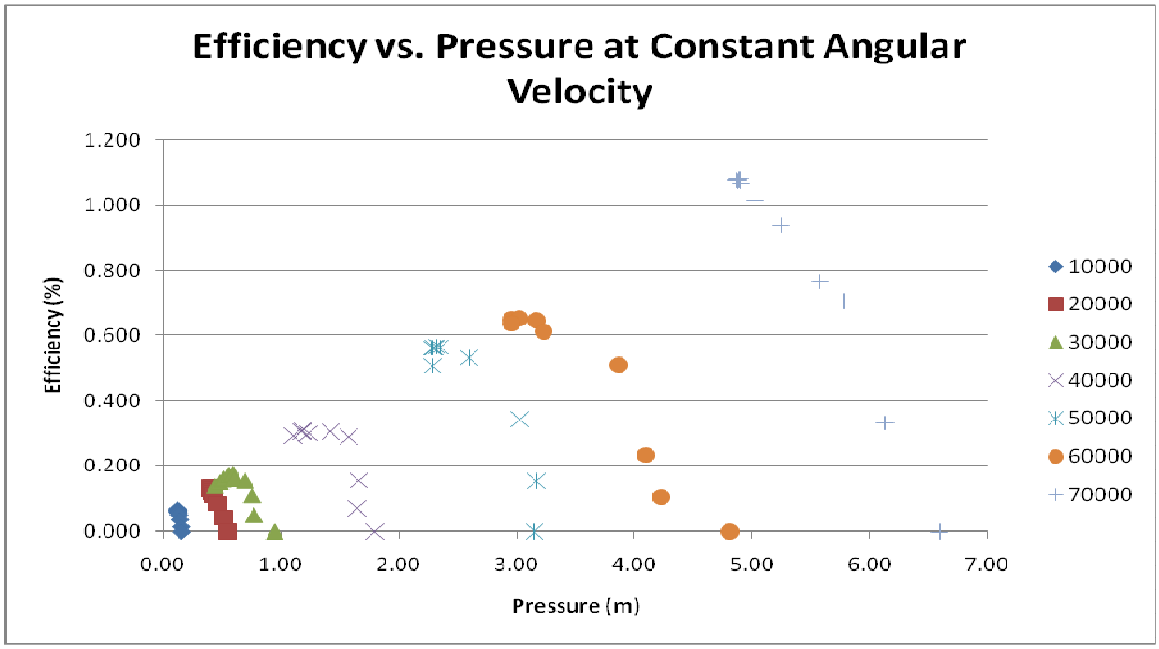

Figure 5.5: Combined Plots of Pump Efficiency versus Pressure.

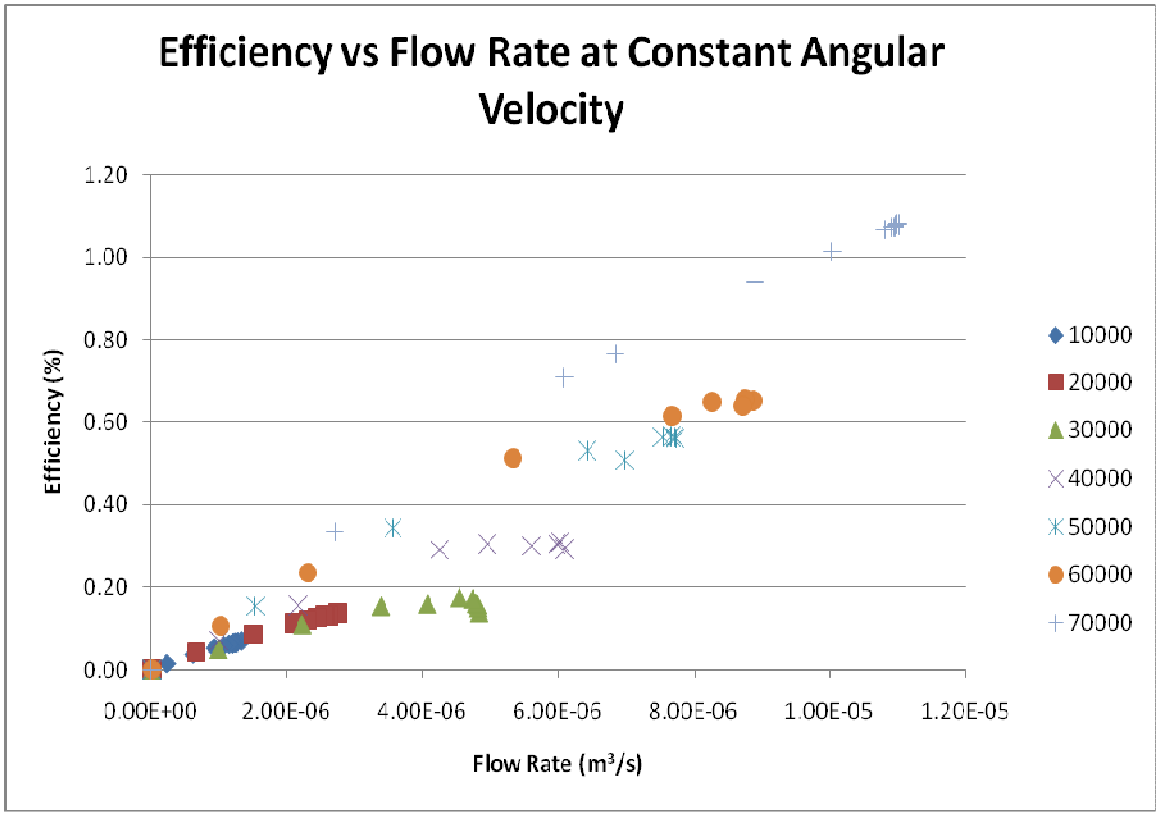

Figure 5.6: Combined Plots of Pump Efficiency versus Flow Rate.

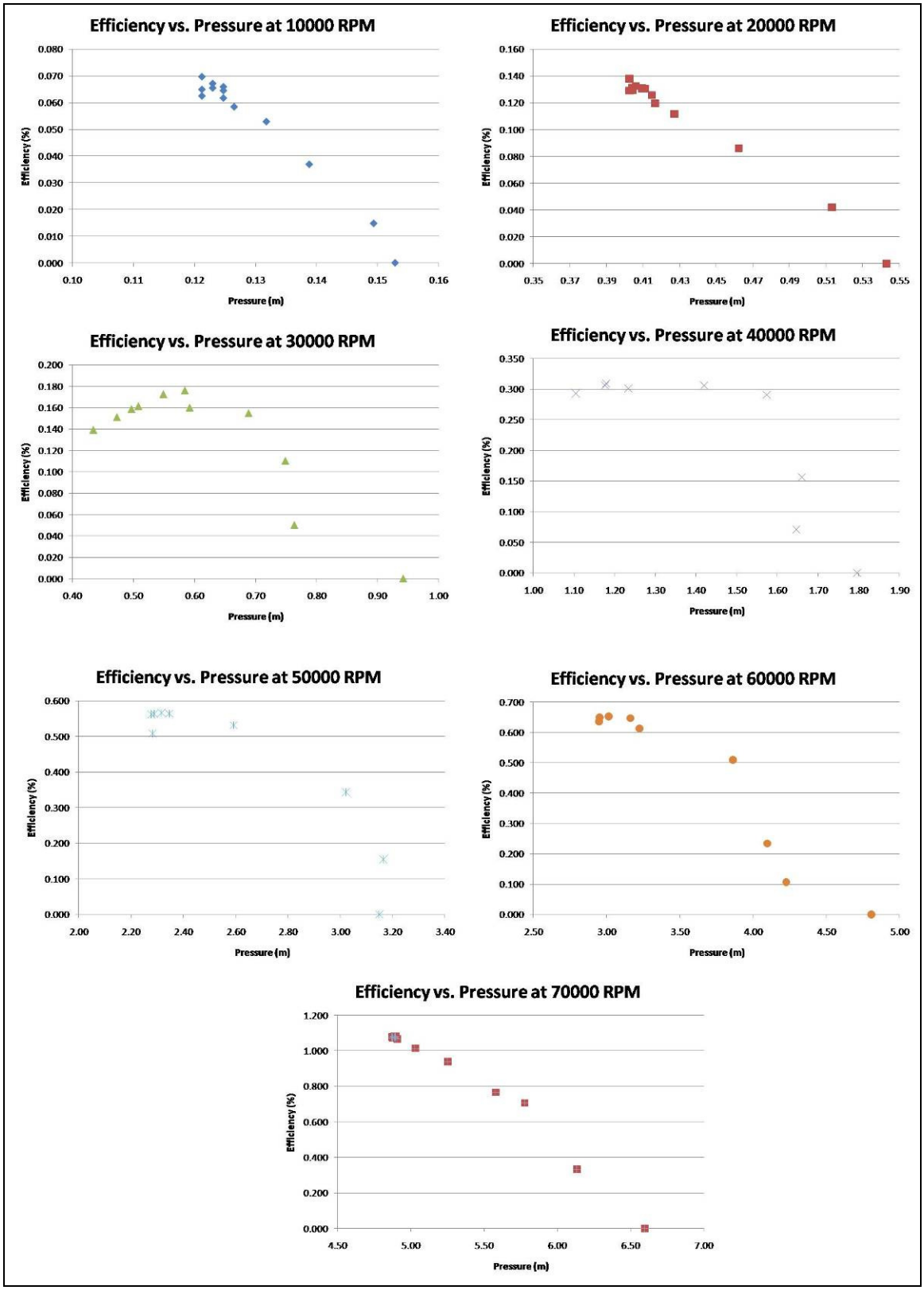

Figure 5.7: Individual Plots of Pump Efficiency versus Pressure.

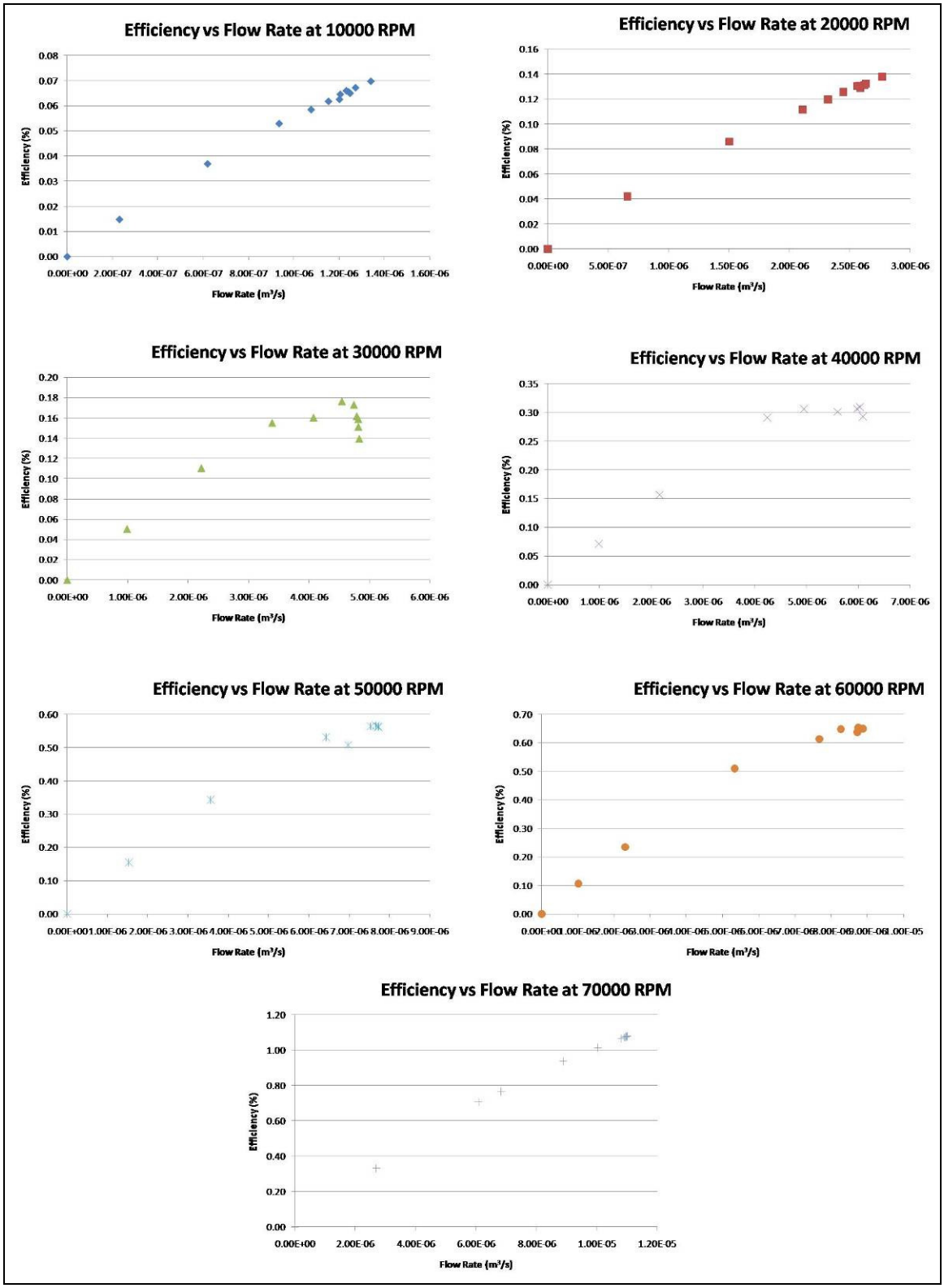

Figure 5.8: Individual Plots of Pump Efficiency versus Flow Rate.

It can be seen that efficiency improves with increasing angular velocity. However, results show that efficiency is only approximately 1.07% at 70000rpm. A curve fit of the actual efficiency versus angular velocity (see Figure 5.9) yields the equation:

$$\eta_{predicted} = 2(10^{-15})\omega^3 + 6(10^{-11})\omega^2 + 5(10^{-7})\omega + 0.0608 \quad (13)$$

The R^2 value of Equation (13) is 0.9803. A generated plot of predicted efficiency and actual efficiency (see figure 5.10) shows the experimental single stage axial flow pump will likely have a maximum predicted efficiency of 24.37% at 220,000rpm. This is well below the expected maximum efficiency of 85%.

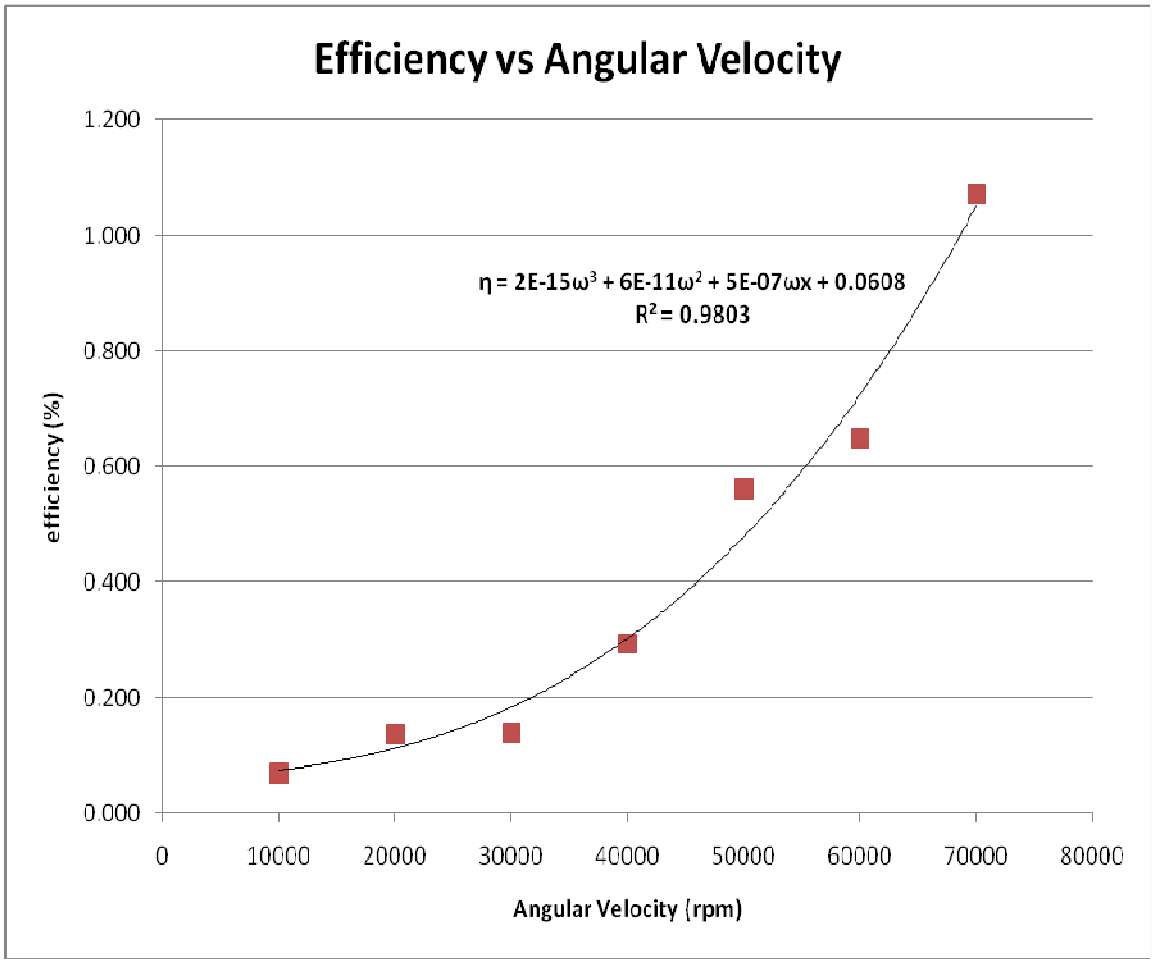

Figure 5.9: Efficiency and Angular velocity Curve Fit.

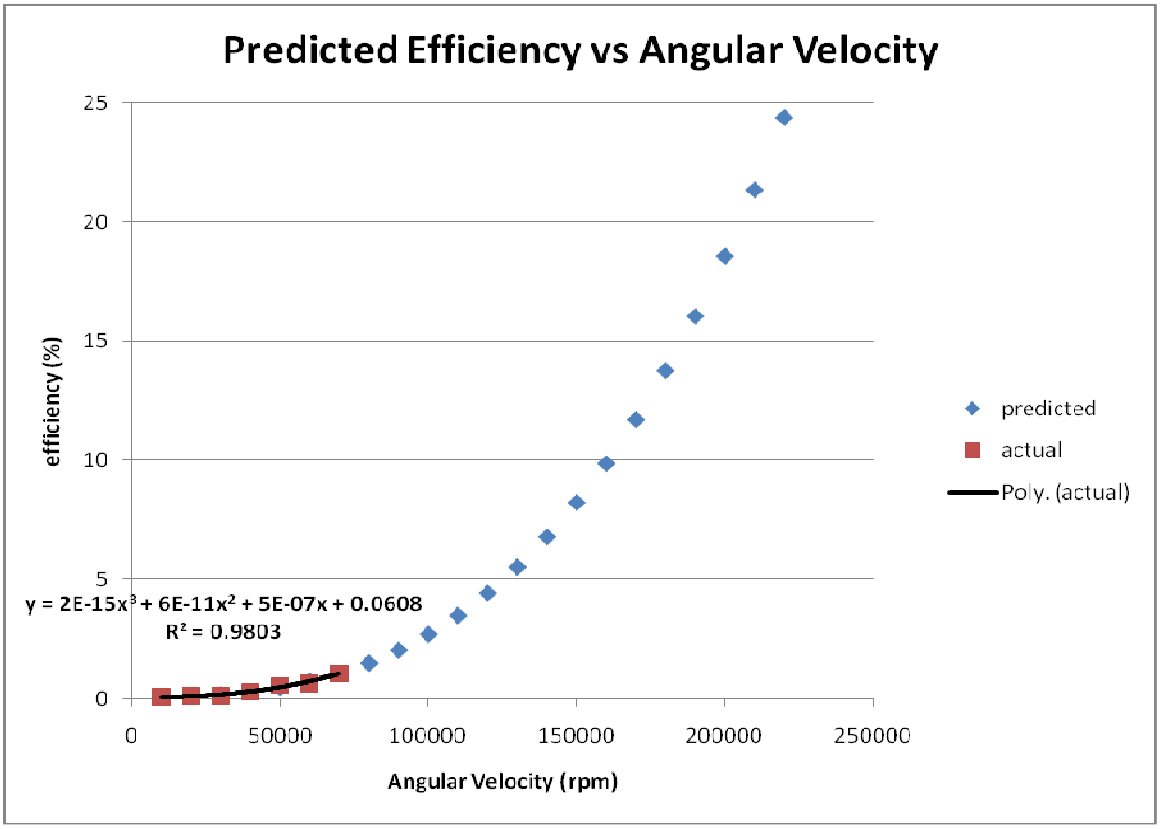

Figure 5.10: Predicted Efficiency as a Function of Angular Velocity.

Chapter 6: Computational Fluid Dynamics

Computational fluid dynamics was used to assist in the analysis of pump performance. The fluid space occupied by the working fluid as it passed through individual pump components was modeled using Unigraphics NX-4 and imported into GAMBIT as parasolids. GAMBIT is a program used to mesh solid bodies in preparation for CFD. In GAMBIT, each component was meshed and all boundaries and surfaces were appropriately defined. Each component consisted of four node tetrahedral elements. Interfaces between components (IGV-rotor and rotor-stator) were defined as mixing zones.

Inherently, the behavior of a pump in operation is unsteady as rotor vanes pass by stationary stator vanes and IGV vanes. Because this is an extremely computationally expensive modeling process, it was in the best interest to consider steady operation of the pump given a long enough period of time. It was also rather difficult to simply model the entire pump and compute fluid flow across all components at the same time. Modeling flow across individual components was used as an alternative approach. The IGV and stator were simplest because no rotation was involved in either component.

Figure 6.1 is a CAD model of the space occupied by fluid in the pump. Cylindrical sections approximately 10mm long were placed ahead of the IGV and after the stator to allow the simulation results to better converge.

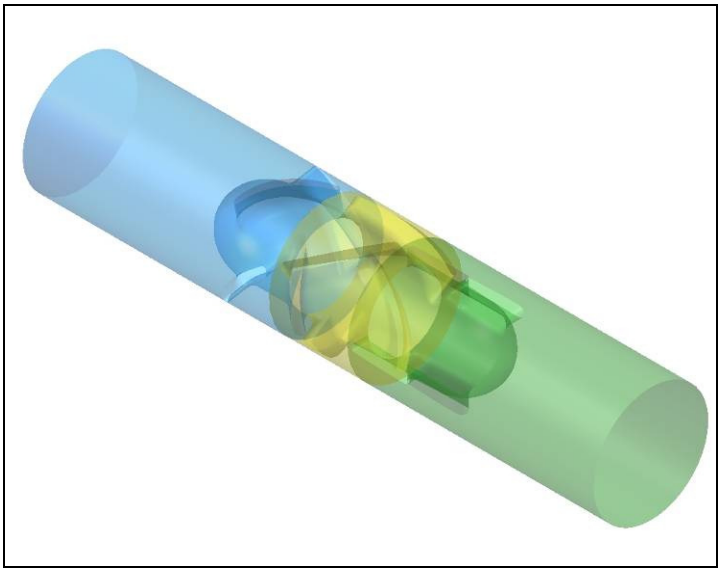

Figure 6.1: CAD Model of Pump Space Occupied By Working Fluid.

6.1 DESCRIPTION OF SOFTWARE

GAMBIT is a software program used to generate meshed of solid bodies and define boundaries. The meshes are then sent to a CFD program for analysis. Meshes are imported into FLUENT for simulations. FLUENT is software program that solves complex fluid dynamics problems. It is especially useful for complex geometries such as the axial flow pump under analysis. In FLUENT, boundary conditions and initial conditions are applied where needed prior to processing.

6.2 MODELING AND PARAMETERS

For all simulations, the realizable κ-ε turbulence modeling was applied and the no slip condition was enforced. The working fluid in all simulations was pure liquid water with a density of 10000kg/m^3 and all pump surfaces were defined as aluminum. Meshes consisted of four-node tetrahedral elements. The IGV consisted of 650,000 elements, the rotor had 254,000 elements, and the stator had 332,000 elements. Only simulations for 30,000rpm pump velocity were conducted. Based on experimental data for single stage axial flow pump at 30,000rpm, the free flow velocity was 0.031m/s. This was the initial velocity set normal to the IGV inlet. Following simulation of the IGV, an area weighted average velocity at the IGV exit was 0.57m/s and was set as the velocity for the rotor inlet. After simulation of the rotor, an area weighted exit velocity at the rotor exit was 0.3m/s. This was set as the stator inlet velocity. All component exits were set as outflow boundaries which allowed the software to solve for conditions at component exits. Up to 1,000 iterations were used for each component simulation.

6.3 CFD RESULTS ANALYSIS

Figure 6.2 shows the velocity vectors along cross-sections perpendicular to the flow direction. In figure 6.3, the pathlines of fluid particles is displayed. Figure 6.4 shows the dynamic pressure contours of each component and Figure 6.5 shows the velocity magnitude contours of each component.

Simulation results show that as the working fluid passes across the vanes of the IGV, it accelerates before entering the rotor. Fluid particle velocity increases going through a region of decreasing cross-sectional area and pressure tends to drop. This can explain why cavitation occurs just past the leading edges of the IGV at angular velocities of 50,000rpm and higher.

The rotor was simulated to rotate at 30,000rpm. Rotor simulations show velocity increases on the inside curve of each vane but only at the latter half. In between vanes, the fluid is does not move very fast by comparison. This is may be due to the spacing of the vanes. The maximum exit velocity of the rotor using an area weighted average was 0.57m/s. The area weighted average velocity after fluid passes the stator is0.44m/s. This would indicate that the stator does not convert the flow energy of the fluid to pressure energy well enough. A possible solution may be the use of a volute chamber.

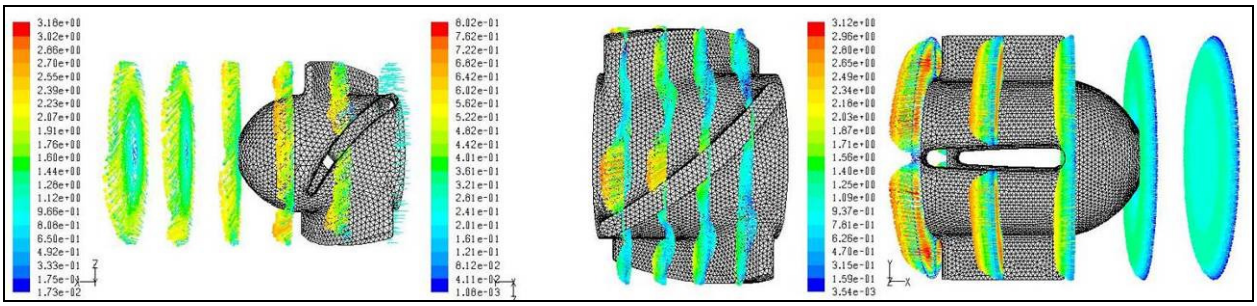

Figure 6.2: CFD Velocity Vectors of Pump Components.

Fluid passing through the stator appears to continue to swirl well past the stator along the inner casing wall but it gradually slows down according to the simulations. This is also evident by seeing the pathlines in Figure 6.3. A total pressure head at the stator exit of 0.16m which does not coincide with the results found during experiments. During experiments, the free flow head at 30,000rpm is 0.43m. It is possible that the pressure (as calculated using CFD) 10mm past the stator are not optimal. A longer distance past the stator may need to be modeled and simulated.

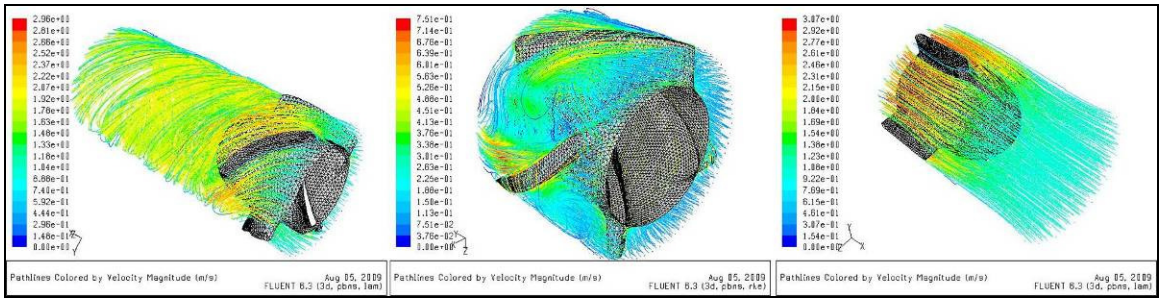

Figure 6.3: Pathlines Colored by Velocity Magnitude.

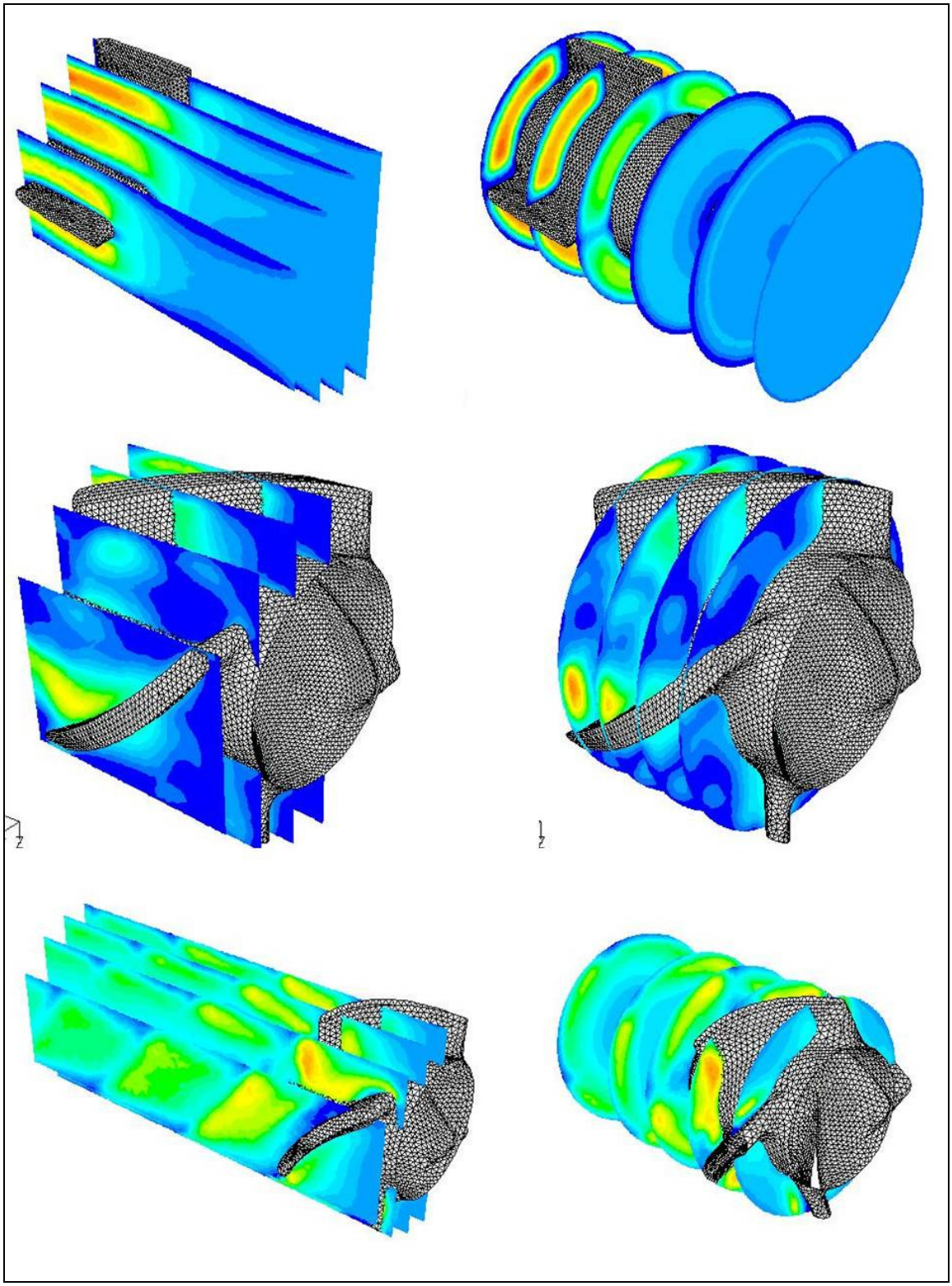

Figure 6.4: Dynamic Pressure Contours of Pump Components.

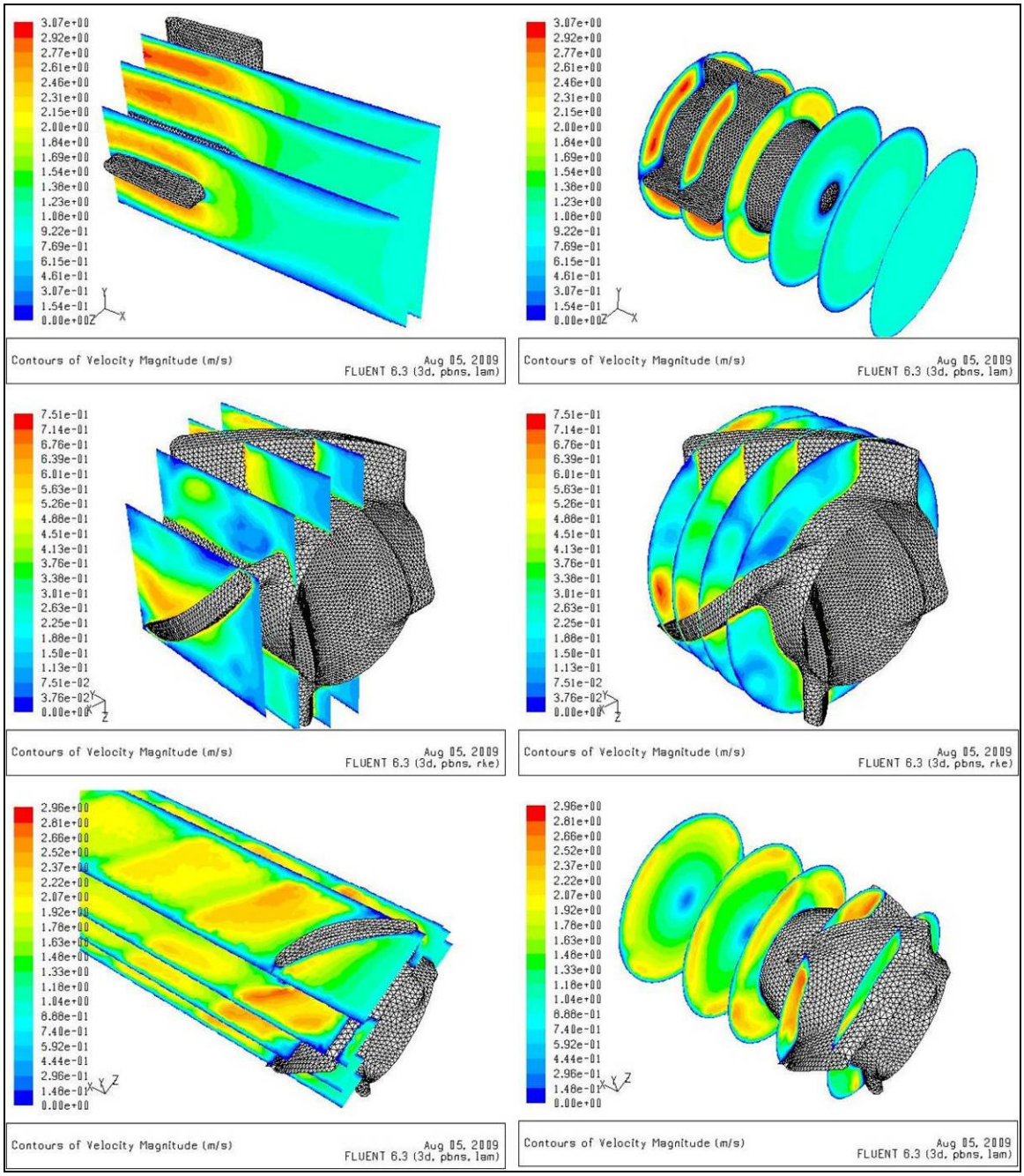

Figure 6.5: Velocity Contours of Pump Components.

Chapter 7: Recommendations and Conclusions

6.1 RECOMMENDATIONS

Future experiments using laser Doppler velocimetry or particle image velocimetry would be useful to map the flow field across the entire pump. A turbine capable of achieving velocities comparable to the intended design specifications of the pump and with sufficient torque should also be developed in order to test the pump up to its maximum design velocity. In order to mitigate cavitation at higher velocities, the suction tank should be pressurized to the maximum designed inlet pressure of 600kPa (6bar). Further evaluations using CFD will help to refine overall pump design as needed.

6.2 CONCLUSIONS

It is possible to determine the pressure and flow characteristics of the experimental axial flow pump using a closed loop system. The single-stage configuration with a volute chamber would be the better option for providing better pressure head. Although this makes the manufacturing process more complicated and thus, more expensive, it may be prudent to further investigate the use of a volute. If better free flow rate is desired, then the choice of a single-stage configuration is best.

Cavitation starts to occur at pump velocities of 50,000rpm. It is not clear if the rotating shaft passing through the IGV plays a factor but it is possible. Further evaluation is needed. Measurements can still be taken but beyond 70,000rpm, data cannot be recorded properly. The reasons are uncertain but vapor bubbles may be affecting measurement devices. Pressurizing the suction tank will help mitigate cavitation.

Efficiency of the pump is 1.07% at 70,000rpm. The resistance in the generator setup circuit is much greater than the frictional resistances of the pump. Since the calculated efficiencies were never much higher than 1%, an alternate method of determining pump efficiency needs to be devised. Current torque measuring technology does not enable torque measurements of the pump because of the extremely small size of the pump.

CFD analysis of the pump operating at 30,000rpm shows that the velocity of the working fluid increases greatly upon passing the IGV vanes and prior to entering the rotor. Rotor simulations show

an increase in fluid velocity but only at the latter half of the vanes. Between vanes, the working fluid does not have much velocity. This may be caused by the wide rotor spacing. It may be necessary to increase the number of rotor vanes, but further modeling and CFD analysis will be needed. The stator does not convert flow energy to pressure energy very well as it can be seen that the fluid continues to swirl well past the stator. It does eventually slow down, but further simulations need to be run in order to determine how far past the stator is pressure optimal.

References

Binder, R.C., 1958, *Advance Fluid Mechanics,* Vol. 1, Englewood Cliffs, NJ: Prentice-Hall, Inc.

Çengel, Yunus A. & Cimbala, John M., 2006, *Fluid Mechanics: Fundamentals and Applications,* New York, NY: McGraw-Hill.

Lecoffre, Yves, 1999, *Cavitation: Bubble Trackers,* Brookfield, VT: A.A. Balkema Publishers.

Nilsson, James W. & Riedel, Susan A., 2005 *Electric Circuits,* 7 ed., Upper Saddle River, NJ: Pearson Prentice Hall.

Round, G. F., 2004, *Incompressible Flow Turbomachines: Design, Selection, Applications, and Theory*, Burlington, MA: Elsevier, Inc.

Stepanoff, A. J., 1993, *Centrifugal and Axial Flow Pump,* 2 ed., Malabar, FL: Krieger Publishing Company.

Turton, R. K., 1994, *Rotodynamic Pump Design,* New York, NY: Press Syndicate of the University of Cambridge.

Curriculum Vita

Jonathon Ray Bice was born on June 13, 1979 in Tacoma Washington to Erik J. Bice and Chun Cha Walker. He was raised in El Paso, Texas and graduated from Andress High School in 1997. Following high school, Jonathon enlisted in the United States Army for four years as an armor crewman on an M1A1 main battle tank. Following his honorable discharge from the Army, Jonathon attended the University of Texas at El Paso to pursue a B.S. in Mechanical Engineering. After three years attending school, he was called back into the military and served in Iraq and Kuwait as part of the Global War on Terror. Upon his return, Jonathon completed his undergraduate degree and immediately began master's studies in mechanical engineering while working as a research assistant in the CPRL. Upon completion of his master's degree, Jonathon will be joining the United States Navy in the highly selective Nuclear Propulsion Officer Candidacy Program. He is happily married to Blanca Margarita Murga-Torres.

Permanent address: 10452 Kendall Street
El Paso, Texas 79924-2442

This thesis was typed by Jonathon R. Bice